



# Infection by phloem-limited phytoplasma affects mineral nutrient homeostasis in tomato leaf tissues

Sara Buoso<sup>a</sup>, Rita Musetti<sup>a</sup>, Fabio Marroni<sup>a</sup>, Alberto Calderan<sup>a,b</sup>, Wolfgang Schmidt<sup>c,d</sup>, Simonetta Santi<sup>a,\*</sup>

<sup>a</sup> Department of Agricultural, Food, Environmental and Animal Sciences, Via delle Scienze 206, University of Udine, 33100, Udine, Italy

<sup>b</sup> Department of Life Sciences, University of Trieste, Via Licio Giorgieri, 5, 34127, Trieste, Italy

<sup>c</sup> Institute of Plant and Microbial Biology, Academia Sinica, 11529, Taipei, Taiwan

<sup>d</sup> Biotechnology Center, National Chung Hsing University, 40227, Taichung, Taiwan

## ARTICLE INFO

### Keywords:

Phytoplasma  
Micro-Tom  
Mineral elements  
RNA-Seq  
Vasculature

## ABSTRACT

Phytoplasmas are sieve-elements restricted wall-less, pleomorphic pathogenic microorganisms causing devastating damage to over 700 plant species worldwide. The invasion of sieve elements by phytoplasmas has several consequences on nutrient transport and metabolism, anyway studies about changes of the mineral-nutrient profile following phytoplasma infections are scarce and offer contrasting results. Here, we examined changes in macro- and micronutrient concentration in tomato plant upon '*Candidatus* Phytoplasma solani' infection. To investigate possible effects of '*Ca. P. solani*' infection on mineral element allocation, the mineral elements were separately analysed in leaf midrib, leaf lamina and root. Moreover, we focused our analysis on the transcriptional regulation of genes encoding trans-membrane transporters of mineral nutrients. To this aim, a manually curated inventory of differentially expressed genes encoding transporters in tomato leaf midribs was mined from the transcriptional profile of healthy and infected tomato leaf midribs. Results highlighted changes in ion homeostasis in the host plant, and significant modulations at transcriptional level of genes encoding ion transporters and channels.

## 1. Introduction

Phytoplasmas are plant pathogenic bacteria causing devastating damage to over 700 plant species worldwide, including many economically important crops, fruit trees, and ornamental plants (Maejima et al., 2014). Phytoplasmas belong to the class *Mollicutes*, a group of wall-less and pleomorphic microorganisms which live a trans-kingdom parasitic life, infecting both plants and phloem-feeding insect hosts (van Bel and Musetti, 2019). In infected plants, phytoplasmas reside in phloem sieve elements and systemically propagate from the site of infection to sink organs (Lee et al., 2021). The nutrient-rich habitat has likely driven the evolution of phytoplasma towards a reduction of the genome, associated with the loss of genes related to essential metabolic pathways. However, these prokaryotes can absorb essential compounds from their hosts via various transporters. Multiple copies of genes associated with the transport of malate, metal-ions, and amino acids are present in the phytoplasma genome (Oshima et al., 2004; Bai et al.,

2006; Kube et al., 2012, 2014). Moreover, phytoplasmas secrete effectors that may directly interact, manipulate, or weaken their hosts (Bai et al., 2009; Hoshi et al., 2009).

The transport of nutrients in the phloem is driven by pressure differences, which are indispensable for the long-distance transport of cues and compounds involved in the response to biotic and abiotic stresses such as peptides, proteins, and other macromolecules, as well as electrical signals, phytohormones, and metabolites (Koenig and Hoffmann-Benning, 2020). The invasion of sieve elements by phytoplasmas has several consequences on nutrient transport and metabolism. In Arabidopsis, phytoplasmas impaired phloem mass flow and carbohydrate transport, probably associated with the plant response, which includes callose deposition at sieve plates and condensation of phloem-protein filaments (Pagliari et al., 2017; Bernardini et al., 2020). In leaves of tomato plants infected with '*Candidatus* Phytoplasma solani' ('*Ca. P. solani*'), phloem hyperplasia and callose deposits at the sieve plates were observed (De Marco et al., 2016, 2021; Buoso et al., 2019).

\* Corresponding author.

E-mail addresses: [sara.buoso@uniud.it](mailto:sara.buoso@uniud.it) (S. Buoso), [rita.musetti@uniud.it](mailto:rita.musetti@uniud.it) (R. Musetti), [fabio.marroni@uniud.it](mailto:fabio.marroni@uniud.it) (F. Marroni), [ALBERTO.CALDERAN@phd.units.it](mailto:ALBERTO.CALDERAN@phd.units.it) (A. Calderan), [wosh@gate.sinica.edu.tw](mailto:wosh@gate.sinica.edu.tw) (W. Schmidt), [simonetta.santi@uniud.it](mailto:simonetta.santi@uniud.it) (S. Santi).

<https://doi.org/10.1016/j.jplph.2022.153659>

Received 18 September 2021; Received in revised form 27 January 2022; Accepted 22 February 2022

Available online 1 March 2022

0176-1617/© 2022 Elsevier GmbH. All rights reserved.

together with a lower rate of exudations of sugars from leaves mediated by the sucrose transporters SUT1 and SUT2 (De Marco et al., 2021). Altered accumulation of amino acids, organic acids, and secondary metabolites have been also reported in phytoplasma-infected plants (Choi et al., 2004; Srivastava et al., 2014; Prezelj et al., 2016).

Mineral nutrients play pivotal roles in the overall plant metabolism and defence processes (Cabot et al., 2019; Thor, 2019). However, studies on mineral-nutrient profile changes following phytoplasma infections are mostly based on analyses of plants grown in field, where it is not possible to control the supply of mineral nutrients (Schweigkofler et al., 2008; Zhao and Liu, 2009; Rossi et al., 2010; Al-Ghaithi et al., 2016). Recently, we demonstrated that in stolbur-diseased tomato plants, 'Ca. P. solani' infection changes iron distribution in tomato leaves, affects the photosynthetic machinery, and perturbs the orchestration of root-mediated transport processes by compromising shoot-to-root communication (Buoso et al., 2019). Tomato plants (cv. Micro-Tom) were grown in hydroponic nutrient solution and infected by grafting. Here, we examine changes in macro- and micronutrient concentration upon 'Ca. P. solani' infection of tomato leaves. To investigate possible effects of 'Ca. P. solani' infection on mineral element allocation, the mineral elements were separately analysed at the leaf midrib and remainder of the leaf (lamina), and in the root. The ionic profile of a specific plant tissue is the result of the activity of several transporters and channels, mediating mineral-elements fluxes within the plant and among different tissues. We focused our analysis on the transcriptional regulation of genes encoding trans-membrane transporters of mineral nutrients. To this aim, a manually curated inventory of differentially expressed genes encoding transmembrane transporters in tomato vasculature was mined from the transcriptional profile (by RNA-seq) of healthy and infected tomato leaf midribs. The transcriptional regulation of transporters implied in fluxes of nutrients, such as  $K^+$ ,  $Ca^{2+}$ ,  $Mg^{2+}$ ,  $Fe^{2+}$  and  $Mn^{2+}$ , has been then reported and discussed in relation to phytoplasma infection in tomato.

## 2. Materials and Methods

### 2.1. Plant material and growth conditions

Tomato (*Solanum lycopersicum* L., cv. Micro-Tom) seeds were collected from fruits of one single plant and germinated for 7 days in the dark at 22 °C between two layers of filter paper soaked in 1 mM  $CaSO_4$ . Homogenous seedlings were transferred into hydroponic nutrient solution containing 1.5 mM  $K_2SO_4$ , 3 mM  $KNO_3$ , 0.5 mM  $MgSO_4$ , 1.5 mM  $CaCl_2$ , 0.5 mM  $NaH_2PO_4$ , 25  $\mu$ M  $H_3BO_3$ , 1  $\mu$ M  $MnSO_4$ , 0.5  $\mu$ M  $ZnSO_4$ , 0.3  $\mu$ M  $CuSO_4$ , 0.05  $\mu$ M  $(NH_4)_6Mo_7O_{24}$ , and 20  $\mu$ M Fe-EDTA. The pH was adjusted to 6.0 with KOH. The aerated nutrient solution was replaced every four days. Plants were grown in a greenhouse at 20–25 °C with a 16 h light photoperiod. After four weeks, half of the plants were infected with 'Candidatus Phytoplasma solani' ('Ca. P. solani'), belonging to the stolbur subgroup 16SrXII-A (Quaglino et al., 2013), by grafting shoot tips from phytoplasma-infected Micro-Tom plants onto healthy plants. Healthy shoot tips were grafted onto the remaining half of the plants. Both leaf and root samples were collected five weeks after grafting. Phytoplasma was detected by RT-PCR as described in De Marco et al. (2016) (Supplemental File 1, Table S1).

### 2.2. Plant biometrics and leaf gas exchange

For biometric analyses and gas exchange measurements, grafted healthy and infected plants were transferred into a growth chamber and grown under a quantum flux density of 250  $\mu$ mol  $m^{-2} s^{-1}$  at the canopy level with a 16 h light photoperiod and an average temperature of 22.5 °C. Biometric analyses were performed five weeks after grafting on at least six plants per condition. Chlorophyll content was indirectly estimated by measuring leaf light transmittance with a portable chlorophyll meter (SPAD-502; Minolta, Osaka, Japan). Five SPAD

measurements were taken on two symptomatic leaves for infected plant, and two corresponding leaves for healthy plant.

Gas exchange measures were taken five weeks after grafting on the terminal leaflet (L) of the more expanded symptomatic leaf (generally L2 or L3, considering L1 the youngest, not completely expanded leaf) of the primary shoot in the infected plants, and the corresponding in healthy plants. Gas exchange parameters were taken with a portable infrared gas analyser LI-6400 XT (LI-COR, Inc., Lincoln, NE, USA). Measurements were made at constant photon flux density (1000  $\mu$ mol  $m^{-2} s^{-1}$ ) during the morning, starting 3 h from the beginning of the light period. Area-based maximum net assimilation ( $A$ ;  $\mu$ mol  $m^{-2} s^{-1}$ ), stomatal conductance ( $g_s$ ;  $mol m^{-2} s^{-1}$ ), intercellular  $CO_2$  concentration ( $C_i$ ;  $\mu$ mol  $mol^{-1}$ ) and leaf transpiration rate ( $E$ ;  $mol m^{-2} s^{-1}$ ) were measured after a stabilization period of about 20 min under ambient concentration of  $CO_2$  (400  $\mu$ mol  $mol^{-1}$ ), a temperature of 25 °C and relative humidity of 50%.

### 2.3. Transmission electron microscopy

To assess the phytoplasma presence in infected plants and the ultrastructural modifications associated with the infection, transmission electron microscopy (TEM) analyses were performed on tomato leaf tissues. To preserve phloem tissue structures, a specifically adapted protocol was used to prepare samples for TEM observation, as reported for tomato (De Marco et al., 2016). Thirty mm long midrib segments were excised from three leaves of five plants per experimental condition. Ultrathin sections (60–70 nm in thickness) were stained with UAR-EMS uranyl acetate replacement stain (Electron Microscopy Sciences, Fort Washington, PA, USA), and observed under a PHILIPS CM 10 (FEI, Eindhoven, The Netherlands) TEM operated at 80 kV, equipped with a Megaview G3 CCD camera (EMSIS GmbH, Münster, Germany). Three non-serial cross sections from each sample were analysed.

### 2.4. ICP-OES analysis

Mineral nutrient concentration (calcium, Ca; copper, Cu; iron, Fe; potassium, K; magnesium, Mg; manganese Mn; sodium, Na; phosphorus, P; sulfur, S; zinc, Zn) were measured in roots and leaves as reported in Buoso et al. (2019). Six plants were analysed for each condition. Leaf midrib and the rest of the leaf (herein called 'lamina') were analysed separately. Root apoplastic Fe pools were removed as described by Bienfait, van den Briel and Mesland-Mul (1985). Briefly, root, midrib and lamina tissues were dried at 65 °C for 48 h, then at 105 °C for 24 h. An aliquot of the samples (200 mg) were acid digested with concentrated  $HNO_3$  [65% (v/v)] using a microwave oven (CEM Mars Xpress Matthews, NC, USA), according to the USEPA 3052 method "Plant Xpress" (USEPA, 1995). Elemental concentration was subsequently determined by Inductively Coupled Plasma–Optical Emission Spectroscopy (ICP-OES, Varian Vista Pro axial). Mineral quantifications were carried out using ICP multi-element standard solution IV (Merck KGaA, Darmstadt, Germany), Phosphorus single-element standard solution and Sulfur single-element standard solution (VWR International). Tomato leaves (NIST SRM 1573a) were used as external certified reference material. Mineral nutrient concentration in leaves was expressed on a dry weight (DW) basis.

### 2.5. RNA-seq

Single-end stranded RNA-seq transcriptome analysis was performed on tomato leaf midribs (cv. Micro-Tom) in a previous experiment (Buoso et al., 2019). Briefly, two leaves from three plants each were pooled and considered as one biological replicate. Three biological replicates for each condition were analysed. Libraries were prepared from 200 ng of total RNA with the TruSeq stranded Total RNA library Prep Plant Kit (Illumina Inc., San Diego, CA, USA), which enables bead-based depletion of ribosomal RNA in multiple plant species. Libraries were sequenced on the Illumina NextSeq500 platform as 75 bp single-end

stranded reads. For each library, more than 45 millions of reads were obtained. Expression pattern of selected differentially expressed genes (DEGs) had previously confirmed the accuracy of RNA-seq data (Buoso et al., 2019). High-quality reads were deposited at NCBI SRA database under BioProject ID: PRJNA548138.

## 2.6. RNA-seq data analysis

After quality evaluation and trimming, clean reads were mapped to the reference genome of the cultivar Heinz 1706, Build SL3.0 and gene annotation ITAG3.20 (release date: June 15, 2017; [https://solgenomics.net/organism/Solanum\\_lycopersicum/genome](https://solgenomics.net/organism/Solanum_lycopersicum/genome)) by TopHat 2.0.9 (Kim et al., 2013), as described in Buoso et al. (2019). DEGs were identified by Cuffdiff 2.1.1 (Trapnell et al., 2013), using multiple-hit correction, min-alignment-count 10, normalization to known transcripts, and a False Discovery Rate (FDR) set to 0.05.

For functional annotation of sequences and data mining, besides the ITAG3.20 annotation from Solgenomics network (SGN), NCBI Entrez was used. Further information on genes was retrieved by aligning all the protein sequences available in the tomato annotation against the NCBI database with the Blastp software (restricted to viridiplantae to reduce computation time), considering matches with an e-value lower than  $10^{-9}$ . The same software was used to identify *Arabidopsis thaliana* homologs. The Kyoto Encyclopedia of Genes and Genomes (KEGG) BRITE Database (<https://www.genome.jp/kegg/brite.html>; Kanehisa et al., 2010) was used to mine from DEGs profiles the genes encoding Transporters (sly02000) (Supplemental File 1, Table S2). Under 'Transporters', secondary transporters comprise two groups: the Solute Carrier Family (SLC), and the Major Facilitator Superfamily (MFS). MFS corresponds to the TC:2.A.1 family in the Transporter Classification Database (TCDB), and classifies electrochemical potential-driven secondary transporters (i.e., symporters, antiporters, and uniporters). The two 'Transporter' groups complete each other and partially overlap. The Sly02000 KEGG BRITE collection includes also primary transporters such as ABC transporters (TC:3.A.1 in TCDB) and proton-translocating diphosphatases (TC:3.A.10), as well as aquaporin and pore ion channels (TC:1 group in TCDB), and electrochemical potential-driven transporters other than MFS members (TC:2 group in TCDB; for example Auxin Efflux Facilitators).

In KEGG database, a few genes related to transport are categorized also under Enzymes as Translocases (sly01000). Translocases catalyzing the translocation of hydrons, inorganic cations or amino acids and peptides and linked to the hydrolysis of a nucleoside triphosphate [EC:7.1.2.-/7.2.2.-/7.4.2.-] that were present just under this category were considered (Supplemental File 1, Table S2). Ion channels (sly04040) were also analysed (Supplemental File 1, Table S3). Several DEGs encoding putative transmembrane transporters according to NCBI annotation but without KEGG assignment (i.e., no KO assigned) were also mined from the DEGs list. To this aim, we analysed several InterPro domains associated to ITAG3.20 proteins (Blum et al., 2020; <https://www.ebi.ac.uk/interpro/>) and combined the related information with the information retrieved by the PANTHER (Protein Analysis Through Evolutionary Relationships) classification system (Mi et al., 2019; <http://www.pantherdb.org/>), the Universal Protein Resource (UniProt, <https://www.uniprot.org/>) and the Transporter Classification Database (TCDB, <http://www.tcdb.org/>) of the *Arabidopsis* homologs. Such a gene list is reported in Supplemental File 1, Table S4.

## 2.7. Statistical analysis

Data are expressed as mean values  $\pm$  SD. Statistical analyses were performed by SigmaPlot 12.0 (SigmaPlot Software, CA, USA), using one-way ANOVA with a Holm-Sidak's test as *post hoc* test for multiple comparisons.

## 3. Results

### 3.1. Phytoplasma infection affects net photosynthesis, stomatal closure, and transpiration

Healthy plants displayed normal growth, while infection significantly affected plant growth and development (Table 1). In infected plants, the typical symptoms of stolbur disease, i.e., leaf yellowing, leaf size reduction, and witches' broom-like proliferations of the shoot occurred 5 weeks after grafting. Altered plant architecture resulted in higher weight of the aerial part (Table 1). Swollen flower buds and malformed, virescent flowers together with almost complete absence of fruits were also observed, confirming previous observations (Buoso et al., 2019). At this stage, phytoplasmas were detected both in leaf midribs and roots (Supplemental File 1, Table S1). Infected plants developed leaf chlorosis and decreased SPAD values, which indirectly estimates the chlorophyll content (Table 1). Measurements of photosynthetic net CO<sub>2</sub> assimilation (A), leaf mesophyll conductance, to which stomatal conductance (g<sub>s</sub>) is the major contributor, intercellular CO<sub>2</sub> concentration (C<sub>i</sub>), and leaf transpiration (E) were made on infected and healthy plants (Fig. 1). Consistently with what was previously observed, phytoplasma infection significantly decreased all these parameters, with the exception of C<sub>i</sub>, for which the observed reduction was not significant.

### 3.2. Microscopic features of phytoplasma-infected plants

TEM observations, performed on midribs of leaves from healthy plants, showed normal cell organization of both sieve elements and companion cells (Fig. 2A, C, E). Numerous, pleomorphic phytoplasma cells were observed in the sieve elements of infected tomato plants (Fig. 2B). Phytoplasma cells showed uneven distribution inside the sieve elements, as they varied in numerosity and disposition (Fig. 2B, F). Some sieve elements appeared filled with phytoplasma cells and collapsed (Fig. 2F). In both healthy and infected samples, the sieve pores at the lateral sieve plates were not constricted by callose collars (Fig. 2A and B). In healthy samples the sieve pores at the ordinary sieve plates were open (Fig. 2C) and surrounded by a layer of callose (Fig. 2C), whereas in infected samples, pores were constricted by callose depositions (Fig. 2D). Regardless of the cell types (i.e., sieve elements, companion cells, or phloem parenchyma cells), cells in the phloem exhibited very thick, convoluted cell walls, confirming previous studies in soil-grown tomato plants (De Marco et al., 2016). Light micrographs of root sections did not reveal any morphological change between healthy and infected roots (Supplemental Fig. S1).

### 3.3. Mineral nutrient concentration is altered by phytoplasma infection

To investigate a possible effect of the infection on the distribution of mineral nutrients, the mineral content of leaves and roots was quantified by ICP-OES. To analyze the allocation of mineral elements inside the leaf, the midrib was cut from the leaf lamina and the two parts were separately analysed.

**Table 1**  
Total plant fresh weight. Results are expressed as mean  $\pm$  SD.

	Healthy	Infected	
Shoot fresh weight (g)	47.1 $\pm$ 4.9	65.6 $\pm$ 6.5	*
Fruit weight (g)	37.3 $\pm$ 9.1	0.9 $\pm$ 1.1	*
Root fresh weight (g)	13.2 $\pm$ 3.4	16.1 $\pm$ 3.4	n.s.
Root max length (cm)	59.2 $\pm$ 17.9	53.4 $\pm$ 12.5	n.s.
SPAD	69.7 $\pm$ 3.8	59.9 $\pm$ 3.6	*

Leaf SPAD index values of fully expanded leaves. Results are expressed as mean  $\pm$  SD.

Asterisks indicate statistically significant differences ( $P < 0.05$ ) among conditions (one-way ANOVA followed by Holm-Sidak's test).

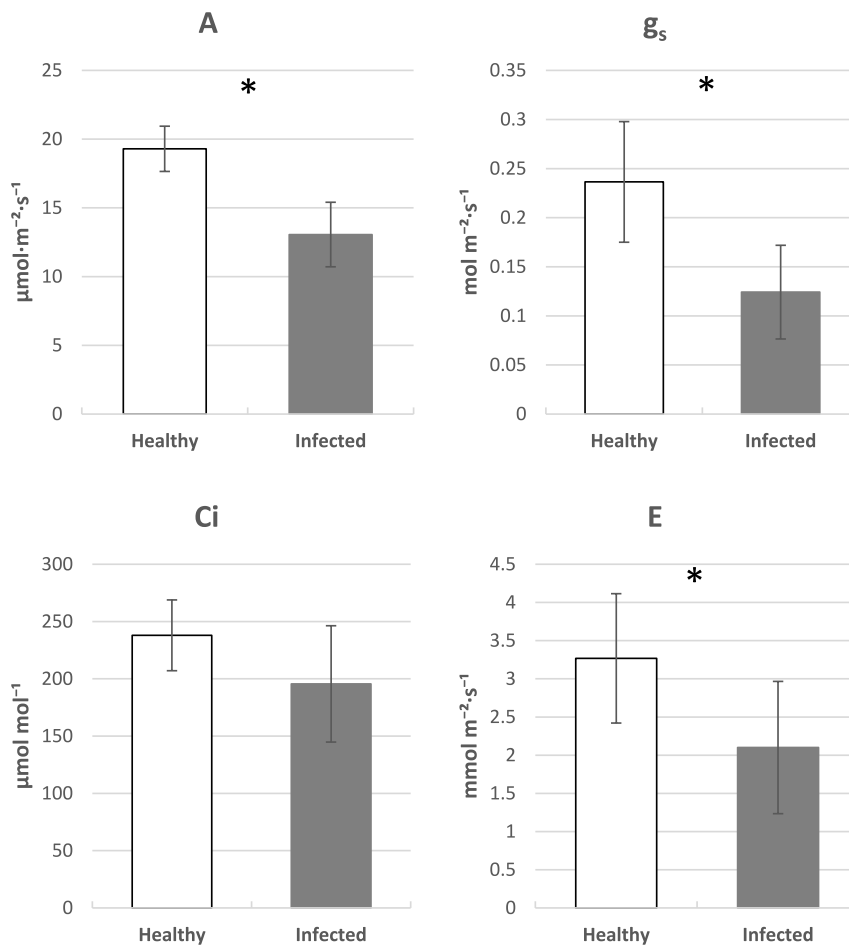


**Fig. 1.** Gas exchange rates. A, area-based maximum net assimilation ( $\mu\text{mol}\cdot\text{m}^{-2}\cdot\text{s}^{-1}$ );  $g_s$ , stomatal conductance ( $\text{mol}\cdot\text{m}^{-2}\cdot\text{s}^{-1}$ );  $C_i$ , intercellular  $\text{CO}_2$  concentration ( $\mu\text{mol}\cdot\text{mol}^{-1}$ ); E, leaf transpiration rate ( $\text{mol}\cdot\text{m}^{-2}\cdot\text{s}^{-1}$ ). All parameters were measured after a stabilization period of about 20 min under ambient concentration of  $\text{CO}_2$  ( $400\mu\text{mol}\cdot\text{mol}^{-1}$ ) and ambient temperature and humidity. Asterisks indicate statistically significant differences ( $P < 0.05$ ) among conditions (one-way ANOVA followed by Holm-Sidak's test).

Among the macronutrients, the analysis revealed altered  $\text{K}^+$  and  $\text{Ca}^{2+}$  concentrations in the midrib of infected leaves. As expected,  $\text{K}^+$  was the most enriched cation in both leaves and roots of tomato plants. In the infected midribs, the  $\text{K}^+$  concentration dropped to about 40% compared to healthy midribs (Fig. 3A). However, in roots,  $\text{K}^+$  levels increased following infection, revealing a possible alteration in the long-distance translocation of  $\text{K}^+$  (Fig. 3A). The  $\text{Na}^+$  concentration was also modified by phytoplasmas, being significant lower in midribs of infected plants relative to healthy midribs. However, the  $\text{K}^+/\text{Na}^+$  ratio, which indicates a possible imbalance in  $\text{K}^+$  homeostasis, was not significantly changed by the pathogen (Fig. 3B). As regards  $\text{Ca}^{2+}$ , its concentration was reduced by the infection in the midrib, while no difference between infected and healthy samples was observed when analyzing the remainder of the leaf (lamina) or the roots. While  $\text{Mg}^{2+}$  levels were similar in healthy and infected midribs, a significant decrease in  $\text{Mg}^{2+}$  concentration was observed in the infected lamina in comparison to healthy lamina. The analysis did not reveal any difference in P and S concentration between infected and healthy plants.

Among the micronutrients under investigation, besides  $\text{Fe}^{2+}$  for which previously higher levels in the infected midribs and lower levels in infected roots were reported (Buoso et al., 2019), only the  $\text{Mn}^{2+}$  concentration was altered by the infection, resulting in an about 40% reduction in the infected midrib (Fig. 3C). A trend towards lower concentrations was also observed in the infected lamina compared to its control, while no difference was determined in roots. The analysis did not reveal any difference in Cu and Zn concentration between infected and healthy plants.

#### 3.4. Phytoplasma infection induces robust expression changes in genes involved in mineral nutrient transport

To gain insights into the transcriptional response of tomato plants to 'Ca. P. solani' infection, we previously performed single-end stranded RNA-seq transcriptome profiling on midrib-enriched leaves (Buoso et al., 2019). Phytoplasma infection altered the expression of a subset of 2773 genes compared to healthy plants ( $\text{FDR} < 0.05$ ). Here, our analysis was focused on the expression changes of genes encoding trans-membrane transport proteins. The transcriptome profile was mined for transport genes using the functional category 'Transporters' (sly02000 for *Solanum lycopersicum*) in the KEGG BRTE database (Supplemental File 1, Table S2). Not included in sly02000, translocases that are catalyzing the translocation of hydrons, inorganic cations or amino acids, and peptides, and are linked to the hydrolysis of a nucleoside triphosphate [EC.7.1.2.-/7.2.2.-/7.4.2.-] were also considered (Supplemental File 1, Table S2). Moreover, ion channels were recovered from KEGG BRTE under sly:04040 (Supplemental File 1, Table S3). By combining information from NCBI RefSeq annotation, InterPro, PANTHER, UniProt and TCDB, we constructed a further list of DEGs encoding putative transmembrane transporters without a KEGG assignment and reported in Supplemental File 1, Table S4.

Phytoplasma infection altered the expression of 191 genes encoding for proteins involved in transmembrane transport, 33 of which are putatively located in cell organelles, representing the 17% of all DEGs. Moreover, a subset of 38 downregulated genes showed dramatic expression changes (from 5- to 282-fold changes).



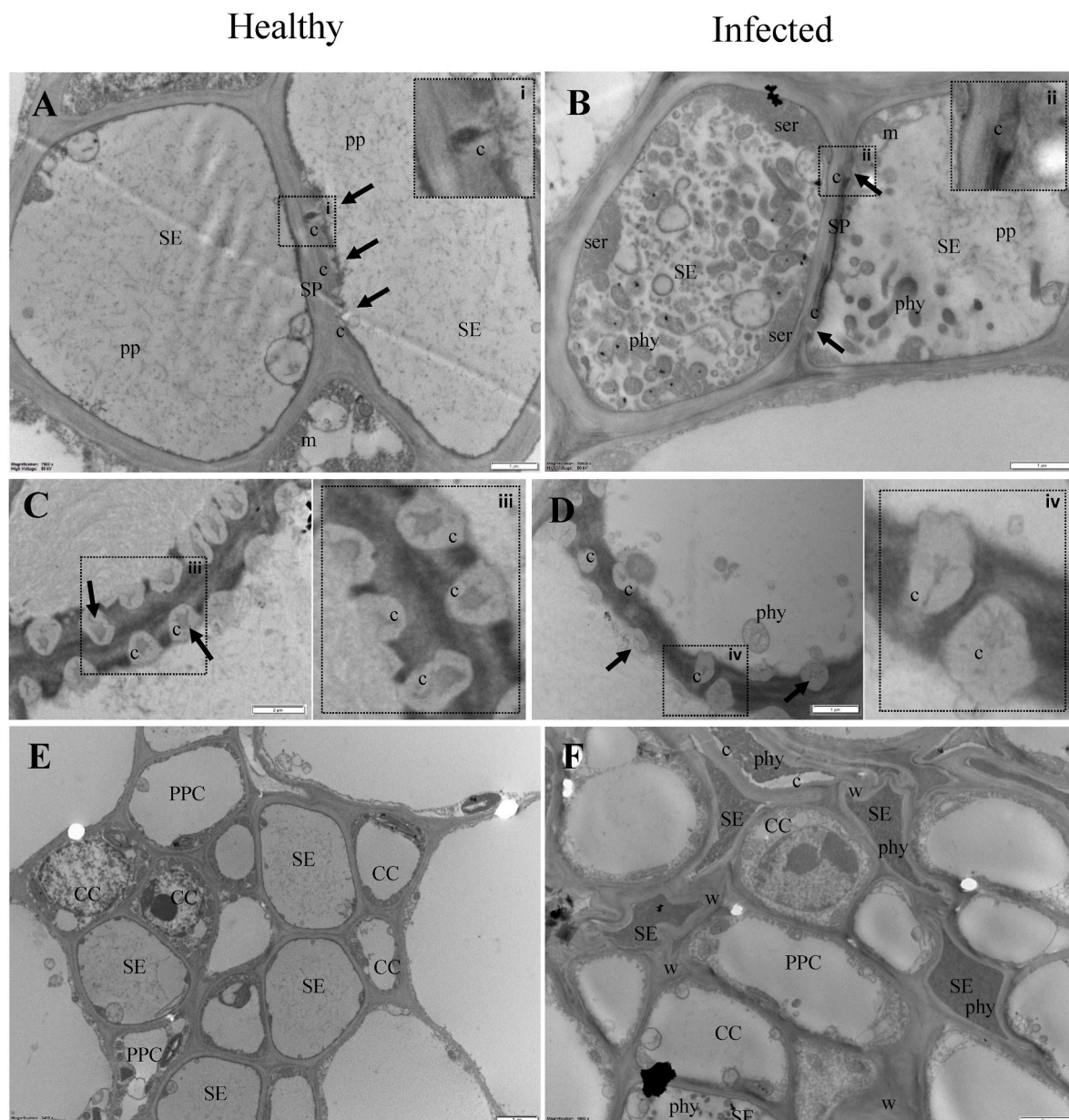


**Fig. 2. Representative cross sections of the phloem in healthy and phytoplasma-infected tomato plants, observed under TEM.** In healthy samples, sieve elements are unaltered and contain protein filaments dispersed in the lumen (A). In infected sieve elements numerous, pleomorphic phytoplasma cells are present. They show uneven distribution, as they vary in numerosity and disposition inside the host cell (B). In both healthy (A) and infected (B) samples, the sieve pores at the lateral sieve plates are not constricted by callose collars, as evidenced in the insets i and ii. In healthy samples the sieve pores at the ordinary sieve plates are open and surrounded by a layer of callose (C and inset iii), whereas in infected samples, pores are constricted by callose depositions (D and inset iv). Phloem of healthy samples (E) presents well-structured sieve elements and companion cells, with a regular shape and no signs of necrosis or subcellular aberrations. In the phloem of infected tomato plants (F), some sieve elements appear filled with phytoplasma cells, contain callose deposits or are collapsed. Regardless of the different phloem cells (i.e. sieve elements, companion cells or phloem parenchyma cells) thick, convoluted cell walls are observed.

c: callose; CC: companion cell; m: mitochondrion; phy: phytoplasmas; PPC: phloem parenchyma cell; SE: sieve element; ser: sieve endoplasmic reticulum; SP: sieve plate; w: cell wall. Arrows in A, B, C and D indicate sieve pores. In A, B and D bars correspond to 1  $\mu\text{m}$ . In C, E and F bars correspond to 2  $\mu\text{m}$ .

### 3.5. Potassium and sodium transport is downregulated in midribs of infected plants

Several low and high-affinity  $\text{K}^+$  transporters and channels have been identified in plants (Very and Sentenac, 2003).  $\text{K}^+$  transporters have been divided into four families, i.e., KT ( $\text{K}^+$  transporter)/HAK (high-affinity  $\text{K}^+$ )/KUP ( $\text{K}^+$  uptake permease), Trk/HKT (High affinity  $\text{K}^+$  transporter), KEA ( $\text{K}^+$  efflux antiporter), and CHX (cation/hydrogen exchanger). Several  $\text{K}^+$  and/or  $\text{Na}^+$  transporters were downregulated in the infected midrib (Table 2, Fig. 4). A schematic representation of  $\text{K}^+$

and  $\text{Na}^+$  transporters and their classification according to the four families is reported in Supplemental Fig. S2. Among high affinity symporters, the most regulated gene was *SIHKT1;2* (Solyc07g014680), which was about ten-fold repressed in infected midribs (Table 2; Supplemental File 1, Table S2). *SIHKT1; 2* is likely localized in the xylem parenchyma cells, and possibly, phloem-associated cells, where modulates  $\text{K}^+/\text{Na}^+$  homeostasis under salinity (Jaime-Pérez et al., 2017).

We found several genes of the CPA superfamily of cation/ $\text{H}^+$  antiporters downregulated. In particular, a member of the cation/proton exchanger (CHX) family of genes (Solyc09g010530; herein called

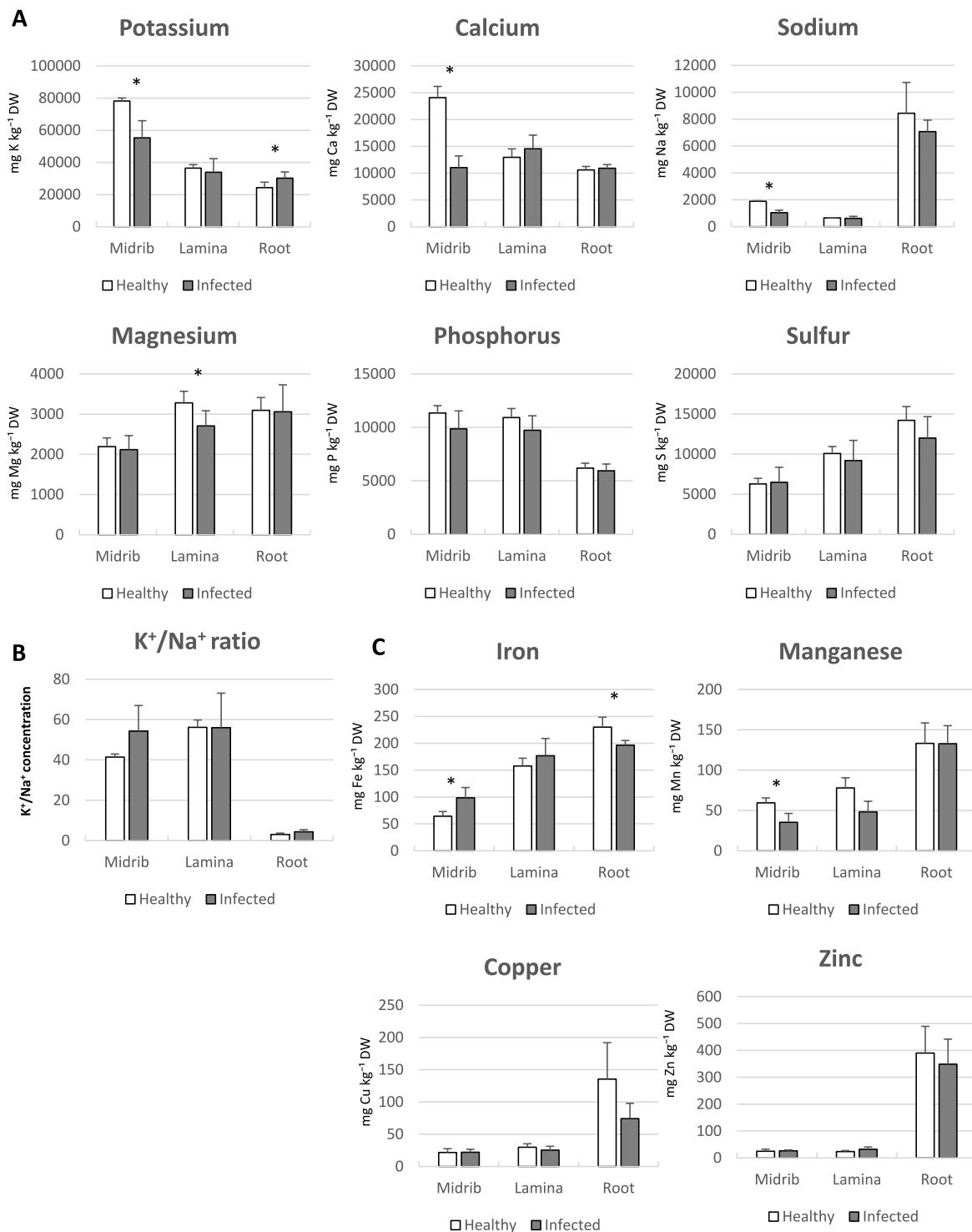


**Fig. 3.** Effects of phytoplasma infection on mineral elements concentration in midribs, laminae and roots. Macronutrients (A) and micronutrients concentration (C) was determined by ICP-OES. K<sup>+</sup>/Na<sup>+</sup> concentration ratio (B). Results are expressed as mean  $\pm$  SD (n = 6). DW: dry weight. Asterisks indicate statistically significant differences (P < 0.05) among conditions (one-way ANOVA followed by Holm-Sidak's test).

*SICHX20*) appeared dramatically repressed (Table 2; Supplemental File 1, Table S4). Similarly, two putatively chloroplast K<sup>+</sup>/H<sup>+</sup> antiporters, Solyc11g044260 and Solyc11g044250 (both aligning to LOC101265888 in NCBI, herein called SIKEA3 like the Arabidopsis K<sup>+</sup> efflux antiporter 3, AtKEA3), were about 5-fold downregulated in infected midribs (Table 2; Supplemental File 1, Table S4). Among K<sup>+</sup>, Na<sup>+</sup>/H<sup>+</sup> exchangers (NHX/NHE exchangers, Saier et al., 2006; Isayenkov et al.,

2020), belonging to a subfamily of the CPA superfamily, the vacuolar LeNHX1 (Solyc06g008820) was also downregulated upon infection.

We included three genes of the NRT1/PTR FAMILY 7.3 family of peptide transporters (Solyc08g077170, Solyc01g080870 and Solyc08g007060) belonging to the AtNRT1.5 group of orthologs. Despite it was originally considered a *bona fide* low affinity transporter of NO<sub>3</sub><sup>-</sup>, AtNRT1.5 has been recently characterized as a proton-coupled H<sup>+</sup>/K<sup>+</sup>

**Table 2**

Genes associated with Potassium and Sodium transmembrane transport.

SGN Locus	Gene description ITAG3.0	NCBI GeneID	Gene description NCBI RefSeq/1st or 2nd blastp hit	Fold- change	Total FPKM	Arabidopsis TAIR 10 Locus tag 1st and 2nd blastp hit
I versus H, DOWNREGULATED						
<b>Solyc09g010530</b>	Cation/H(+) antiporter (CHX)	101249848	cation/H(+) antiporter 20	282.5	40.5	AT3G53720   ATCHX20, CHX20   cation/ H+ exchanger 20; AT3G17630   ATCHX19, CHX19   cation/ H+ exchanger 19 AT1G32450   NRT1.5   nitrate transporter 1.5; AT4G21680   NRT1.8   NITRATE TRANSPORTER 1.8 AT1G32450   NRT1.5   nitrate transporter 1.5; AT4G21680   NRT1.8   NITRATE TRANSPORTER 1.8
<b>Solyc08g077170</b>	Peptide transporter, putative (PTR)	101263538	protein NRT1/PTR FAMILY 7.3	42.5	19.9	AT1G32450   NRT1.5   nitrate transporter 1.5; AT4G21680   NRT1.8   NITRATE TRANSPORTER 1.8
<b>Solyc01g080870</b>	Peptide transporter, putative (PTR)	101250924	protein NRT1/PTR FAMILY 7.3	13.3	152.0	AT1G32450   NRT1.5   nitrate transporter 1.5; AT4G21680   NRT1.8   NITRATE TRANSPORTER 1.8
<b>Solyc07g014680</b>	sodium transporter HKT1; 2	101251695	sodium transporter HKT1; 2	10.1	34.1	AT4G10310   HKT1, ATHKT1   high- affinity K+ transporter
<b>Solyc11g044260</b>	K(+) efflux antiporter (KEA)	101265888	ref XP_004250822.1 K(+) efflux antiporter 3, chloroplastic	5.3	35.8	AT4G04850   KEA3, ATKEA3  K+ efflux antiporter 3
<b>Solyc11g044250</b>	K(+) efflux antiporter (KEA)	101265888	ref XP_004250822.1 K(+) efflux antiporter 3, chloroplastic	5.0	28.0	AT4G04850   KEA3, ATKEA3  K+ efflux antiporter
<b>Solyc08g007060</b>	Peptide transporter, putative (PTR)	101257685	protein NRT1/PTR FAMILY 7.3	3.3	8.7	AT1G32450   NRT1.5   nitrate transporter 1.5; AT4G21680   NRT1.8   NITRATE TRANSPORTER 1.8
<b>Solyc05g051220</b>	Potassium channel TORK1	101261922	potassium channel SKOR-like	3.2	2.0	AT3G02850   SKOR   STELAR K+ outward rectifier; AT5G37500   GORK   gated outwardly- rectifying K+ channel
<b>Solyc08g081810</b>	Cation/H(+) antiporter (CHX)	101267631	cation/H(+) antiporter 18-like	3.2	2.3	AT5G41610   ATCHX18, CHX18   cation/ H+ exchanger 18; AT4G23700   ATCHX17, CHX17   cation/ H+ exchanger 17
<b>Solyc08g015680</b>	Potassium transporter (KUP/HAK/KT)	101251111	potassium transporter 4-like	3.0	10.9	AT3G02050   KUP3, ATKUP3, ATK4  K+ uptake transporter
<b>Solyc06g008820</b>	Na+/H+ antiporter 1 (NHX)	543771	NHX1; Na+/H+ antiporter, isoform 1	1.9	10.4	AT3G05030   NHX2, ATNHX2   sodium hydrogen exchanger; AT5G27150   NHX1, ATNHX, AT-NHX1, ATNHX1   Na+/H+ exchanger
<b>Solyc02g087000</b>	Potassium transporter (KUP/HAK/KT)	101248158	ref XP_004232287.1  PREDICTED: potassium transporter 8-like	1.7	49.9	AT5G14880   KUP8   Potassium transporter family protein; AT1G70300   KUP6  K+ uptake permease 6

Fold-change is the expression level ratio Infected/Healthy. Total FPKM corresponds to the sum of FPKM expression of the corresponding gene in both samples. In italic, different SGN loci corresponding to the same Gene ID in NCBI annotation. In brackets: symbol of transporter family.

antiporter that mediates the transport of K<sup>+</sup> into the xylem (Li et al., 2017).

Regarding K<sup>+</sup> fluxes mediated by selective channels, only one K<sup>+</sup> outward channel (SKOR-like, Solyc05g051220) was transcriptionally downregulated in the infected midribs when compared to the control, although expressed to a very low level, (Table 2; Supplemental File 1, Table S2). A schematic overview of the changes in K<sup>+</sup> and Na<sup>+</sup> transport (and Ca<sup>2+</sup>, see below) following phytoplasma infection is depicted in Fig. 4.

### 3.6. Aquaporins and small neutral solute transporters

In the midrib of infected leaves, several K<sup>+</sup> transporters and Na<sup>+</sup> exchangers were found to be repressed. It is well-established that K<sup>+</sup> fluxes are coupled to the activity of water channels/aquaporins in the plasma membrane (PIPs: plasma membrane intrinsic proteins). PIPs belong to the Major Intrinsic Proteins (MIP) family (TC 1.A.8; Saier et al., 2006; Reuscher et al., 2013). Several MIP genes were downregulated in the infected leaf midribs (Table 3; Supplemental File 1, Tables S2 and S4). Among the five modulated genes encoding PIPs, two genes encoding PIP2-1 (Solyc09g007765 and Solyc09g007760) were the most repressed, whereas PIP1-5 (Solyc08g081190) the most robustly expressed. Similar to what was observed for PIPs, two genes encoding tonoplast aquaporins (TIPs; Reuscher et al., 2013) were repressed in infected plants (Solyc12g044330, TIP2-1, and Solyc03g120475,

TIP2-2). Two members of the uncategorized X intrinsic protein (XIP; Reuscher et al., 2013) subfamily were repressed, whereas a small, basic intrinsic proteins (SIP) member was upregulated.

### 3.7. Calcium transport

The strongest effect of the phytoplasma infection was observed with regard to changes in the calcium concentration, as reported above. In plants, Ca<sup>2+</sup>-permeable channels, Ca<sup>2+</sup>-ATPases, and Ca<sup>2+</sup>/cation antiporters (CaCA) mediate Ca<sup>2+</sup> fluxes and maintain cytosolic Ca<sup>2+</sup> homeostasis. We found that several genes encoding both calcium channels and transporters were differentially regulated following phytoplasma infection (Table 4; Supplemental File 1, Tables S2, S3, S4). A schematic representation of genes mediating Ca<sup>2+</sup> transport is depicted in Supplemental Fig. S3.

The CaCA superfamily comprises at least five gene families: Na<sup>+</sup>/Ca<sup>2+</sup> exchanger (NCX), Na<sup>+</sup>/Ca<sup>2+</sup>, K<sup>+</sup> exchanger (NCKX), H<sup>+</sup>/cation exchanger (CAX), YRBG, and cation/calcium exchanger (CCX) family (Cai and Lyttton, 2004). A Na<sup>+</sup>/Ca<sup>2+</sup> exchanger (Solyc03g006260) was 3-fold upregulated in the infected midribs (Table 4; Table S4). Its Arabidopsis homolog, AtNCL, mediates Ca<sup>2+</sup> efflux and Na<sup>+</sup> uptake into vacuolar vesicles and is regulated by [Ca<sup>2+</sup>]<sub>cyt</sub>, having Ca<sup>2+</sup>-binding activities. Conversely, two vacuolar Ca<sup>2+</sup>/H<sup>+</sup> antiporters belonging to the CAX family (Solyc06g006110 and Solyc09g005260) were downregulated, together with SLCX1 gene, a cation/Ca<sup>2+</sup> antiporter

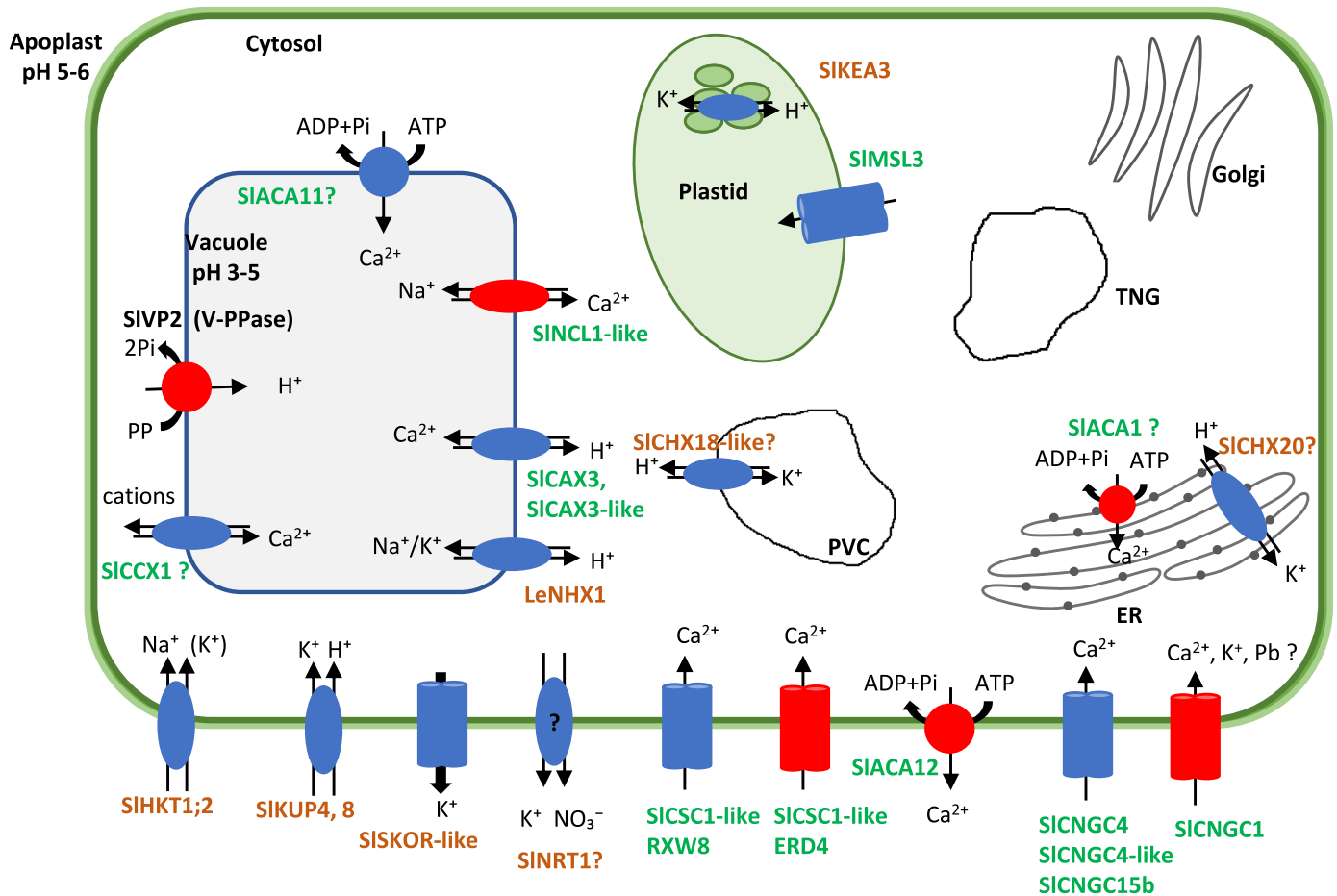


**Fig. 4.** A schematic overview of cellular localization and transport mechanism of the  $K^+$  and  $Ca^{2+}$  transporters, pumps and channels up- and downregulated upon phytoplasma infection.  $K^+$  (orange lettering) and  $Ca^{2+}$  (green lettering) pumps (circles), transporters (ellipses) and channels (cylinders) are displayed in a hypothetical tomato leaf cell. For the complete gene annotation refer to Tables 2 and 4. The question mark indicates a *bona fide* localization of the transporter based on the localization of the *Arabidopsis* homolog. In red: up-regulated genes; in blue: down-regulated genes.

ER, Endoplasmic reticulum; PVC, prevacuolar compartment; TGN, trans-Golgi network; CHX, cation/ $H^+$  exchanger; KEA,  $K^+$ -efflux antiporter; NHX (NHE),  $Na^+/H^+$  exchanger; V-PPase,  $H^+$ -translocating pyrophosphatase; HKT, High-affinity  $K^+$  transporter; NRT, nitrate transporter; SKOR,  $K^+$  outward rectifier; KUP,  $K^+$  uptake transporter; CAX,  $Ca^{2+}/H^+$  exchanger; ACA, autoinhibited calcium ATPase; NCL (NCX),  $Na^+/Ca^{2+}$  exchanger; CCX, cation/ $Ca^{2+}$  exchanger; MSL, mechanosensitive ion channel; CNGC, cyclic nucleotide gated ion channel; CSC1-like, OSCA/TMEM63 stress-gated cation channel. (For interpretation of the references to colour in this figure legend, the reader is referred to the Web version of this article.)

(Table 4; Table S1).

In *Arabidopsis*,  $Ca^{2+}$  is transported into the mesophyll vacuoles by ACA11, an auto-inhibited  $Ca^{2+}$ -ATPase (ACA; Bonza and De Michelis, 2011) that is homolog to Solyc10g079300, a putative calcium-transporting ATPase which was downregulated in infected midribs, thus suggesting a reduced flux of  $Ca^{2+}$  into the vacuole in infected leaves (Table 4; Table S2). Consistently, two other  $Ca^{2+}$ -ATPases, Solyc02g090560 and Solyc04g077870 (plasma membrane and likely endoplasmic reticulum  $Ca^{2+}$ -ATPase, respectively), were upregulated under the same condition, indicating a possible higher flux of  $Ca^{2+}$  into cell compartments different from vacuole and/or toward the apoplast (Table 3; Table S2).

Regarding ion channels, two CSC1-like proteins (Solyc08g023440 and Solyc12g088230) of the conserved OSCA/TMEM63 family of  $Ca^{2+}$  permeable stress-gated cation channels were up- and downregulated, respectively (Table 4; Table S2). *Arabidopsis* CSC1 is a non-rectifying, plasma membrane-bound, calcium-permeable, and stress-gated cation channel, activated by hyperosmotic shock (Hou et al., 2014). A third, chloroplast-localized channel (Solyc04g076303) belonging to the large family of mechanosensitive channels that provide protection against hypo-osmotic shock, was downregulated (Table 4; Table S2). Moreover, members of a class of channels referred to as CNGC (cyclic nucleotide

gated channels) appeared to be transcriptionally regulated in infected leaves. Three genes encoding CNGCs were downregulated (Table 3; Tables S3 and S4). A schematic overview of the changes in  $K^+$  and  $Na^+$  transport and  $Ca^{2+}$  following phytoplasma infection is depicted in Fig. 4.

### 3.8. Magnesium transporters

Magnesium content remained unchanged in midribs, while  $Mg^{2+}$  levels decreased in the lamina portion, as reported above (Fig. 3). However, genes encoding  $Mg^{2+}$  transporters were downregulated in the infected midribs; the most important gene expression changes were relieved at the chloroplast, indicating an altered  $Mg^{2+}$  loading into this organelle (Table 5; Table S1).

### 3.9. Manganese and iron transport

We previously showed that  $Fe^{2+}$  shifts to the phloem tissue from the surrounding tissue in the phytoplasma-infected tomato leaves (Buoso et al., 2019). In this work, the analysis of microelements revealed a significant imbalance of the  $Fe^{2+}/Mn^{2+}$  ratio in the infected midrib, due to increased  $Fe^{2+}$  and decreased  $Mn^{2+}$  concentrations (Fig. 3). Thus, we focused on the transcriptional regulation of genes putatively responsible



**Table 3**  
Genes belonging to Major Intrinsic Protein (MIP) family (TC 1.A.8).

SGN Locus	Gene description ITAG3.0	NCBI Gene ID	Gene description NCBI RefSeq/ 1st or 2nd blastp hit	Fold- change	Total FPKM	Arabidopsis TAIR 10 Locus tag 1st and 2nd blastp hit
I versus H, UPREGULATED						
<b>Solyc10g078490</b>	ripening-related mRNA	101244430	aquaporin SIP1-2-like	1.8	15.6	AT5G18290 SIP1; 2   Aquaporin-like superfamily protein
I versus H, DOWNREGULATED						
<b>Solyc09g007765</b>	Aquaporin-like protein (PIP)	101247747	ref[NP_001289823.1] aquaporin PIP2-1	14.4	52.0	AT3G53420   PIP2A, PIP2, PIP2; 1   plasma membrane intrinsic protein
<b>Solyc09g007760</b>	plasma membrane intrinsic protein 2.10 (PIP)	101247747	ref[NP_001289823.1]aquaporin PIP2-1	11.0	65.6	AT3G53420   PIP2A, PIP2, PIP2; 1   plasma membrane intrinsic protein
<b>Solyc10g054820</b>	X-intrinsic protein 1.2 (XIP)	101251423	Aquaporin-5	9.7	11.6	AT4G00430   TMP-C, PIP1; 4, PIP1E   plasma membrane intrinsic protein; AT1G01620   PIP1C, TMP-B, PIP1; 3   plasma membrane intrinsic protein
<b>Solyc08g081190</b>	plasma membrane intrinsic protein 1.5 (PIP)	544086	PIP1-5, plasma membrane intrinsic protein 1.5	3.5	1570.4	AT4G00430   TMP-C, PIP1; 4, PIP1E   plasma membrane intrinsic protein
<b>Solyc01g111660</b>	plasma membrane intrinsic protein 2.8 (PIP)	101268623	plasma membrane intrinsic protein 2.8	2.6	92.1	AT4G35100   PIP3 or PIP3, PIP3A, PIP2; 7, SIMIP   plasma membrane intrinsic protein
<b>Solyc12g044330</b>	tonoplast intrinsic protein 2.1 (TIP)	101245626	ref[NP_001289845.1] aquaporin TIP2-1	2.4	98.3	AT3G16240   DELTA-TIP, TIP2; 1, DELTA-TIP1, AQP1, ATTIP2; 1; AT5G47450   ATTIP2; 3, TIP2; 3, DELTA-TIP3   tonoplast intrinsic protein
<b>Solyc06g011350</b>	plasma membrane intrinsic protein 2.4 (PIP)	100529106	aquaporin	2.3	10.8	AT2G37170   PIP2B, PIP2; 2   plasma membrane intrinsic protein; AT3G53420   PIP2A, PIP2, PIP2; 1   plasma membrane intrinsic protein
<b>Solyc10g054840</b>	X-intrinsic protein 1.1 (XIP)	100750254	X intrinsic protein	1.9	8.6	AT4G23400   PIP1D, PIP1; 5   plasma membrane intrinsic protein 1; 5; AT1G01620   PIP1C, TMP-B, PIP1; 3   plasma membrane intrinsic protein
<b>Solyc03g120475</b>	Tonoplast intrinsic protein, putative (TIP)	101055566	TIP2-2, tonoplast intrinsic protein 2.2	1.6	286.7	AT3G16240   DELTA-TIP, TIP2; 1, DELTA-TIP1, AQP1, ATTIP2; 1; AT5G47450   ATTIP2; 3, TIP2; 3, DELTA-TIP3   tonoplast intrinsic protein

DEGs belong to the aquaporins subfamilies PIPs (plasma membrane intrinsic proteins), TIPs (tonoplast intrinsic proteins), SIPs (small, basic intrinsic proteins) and XIPs (uncategorized X intrinsic protein) according to [Reuscher et al. \(2013\)](#). Among PIPs, PIP2s are known to possess more water transport capacity than PIP1s, but PIP1s may increase the activity of PIP2s by forming heterotetramers ([Fetter et al., 2004](#)). Fold-change is the expression level ratio Infected/Healthy ( $q \leq 0.05$ ). Total FPKM corresponds to the sum of FPKM expression level of the corresponding gene in both samples. In italic, different SGN loci corresponding to the same Gene ID in NCBI annotation. In brackets: symbol of transporter family. Both Solyc09g007765 and Solyc09g007760 proteins significantly aligned with PIP2-1, encoded by Gene ID 101247747 in NCBI annotation, although Solyc09g007760 was annotated as PIP2; 10 by Reuscher et al. (2013).

for the transmembrane transport of these metals ([Table 6; Tables S1 and S4](#)).  $Mn^{2+}$  and  $Fe^{2+}$  are essential metal nutrients, but are also extremely reactive and able to generate harmful, reactive oxygen species if mal-distributed or accumulated in excess amounts. Only a small portion of both minerals is present as free metal in the cell, mainly in the vacuole, the major part functions as cofactor or complexed by various ligands. We found that only a few genes encoding metal ion transporters were regulated in the infected midrib, and only one known transporter of metal–nicotianamine (NA) chelates ([Table 6; Tables S1 and S4](#)). A natural resistance-associated macrophage protein (NRAMP) transporter (Solyc03g116900; NRAMP6) was downregulated, as well as four different genes, all encoding putative metal transporters targeted to organelles. On the other hand, two genes were upregulated in the infected midrib: a Metal Tolerance Protein (MTP 4-like; Solyc01g006150) and a yellow stripe-like (YSL) gene (Solyc03g082620; YSL2). MTPs (also called CDF: Cation Diffusion Facilitator) are specific for  $Mn^{2+}$  transport; AtMTP8 is a tonoplast  $Mn^{2+}$  transporter ([Peiter et al., 2007](#)).

**4. Discussion**

**4.1. Phytoplasma infection affects net photosynthesis, stomatal closure, and transpiration**

Proliferations of vegetative tissues (witches’ broom-like proliferation of the shoot) and smaller leaves, associated to reduction in chlorophyll content resulting in leaf chlorosis, yellowing and lower net photosynthesis together with a gradual decrease of transpiration, are common

outcomes of the infection by phytoplasmas ([Bertamini and Nedunchezian, 2001; Endeshaw et al., 2012; Vitali et al., 2013; Buoso et al., 2019](#)). We revealed that infection affected stomatal conductance in tomato, confirming what observed in Flavescence dorée-as well as Bois noir-diseased grapevine plants ([Vitali et al., 2013; Endeshaw et al., 2012](#)). In phytoplasma-infected grapevine, stomatal closure was associated with high internal  $CO_2$  concentrations, suggesting metabolic, non-stomatal limitation to carbon assimilation ([Vitali et al., 2013](#)). However, decreased photosynthetic capacity is not always associated with a stomatal response, arguing against a mechanistic link between the two processes ([von Caemmerer et al., 2004](#)). Stomatal movements rely on turgor and volume changes in the guard cells, and the main solutes involved in their osmoregulation are  $K^+$  and sucrose, which move across the membrane together with counter-anions such as chloride, nitrate, sulfate, and malate ([Talbot and Zeiger, 1998](#)). Both  $K^+$  and sucrose are primary guard cell osmotica with either substance dominating in two distinct phases:  $K^+$  accumulation drives the rapid stomatal opening, while turgor maintenance depends on the following sucrose-dominated phase ([Talbot and Zeiger, 1998](#)). Sucrose accumulation in the apoplast of guard cells was proposed to account for stomata closure ([Lu et al., 1997; Outlaw, 2003](#)). Indeed, anomalous sucrose and starch accumulation were observed in phytoplasma-infected periwinkle, grapevine, and tomato leaves ([Lepka et al., 1999; Musetti et al., 2007; Santi et al., 2013a,b; De Marco et al., 2021](#)), together with altered sucrose transport and metabolism ([Santi et al., 2013a,b; De Marco et al., 2021](#)). However,  $K^+$  is highly mobile and energetically economic, supporting its accumulation in the guard cell vacuole to drive stomatal opening ([MacRobbie, 2006](#)). An uphill  $K^+$  transport into the vacuole is

**Table 4**  
Genes mediating Calcium fluxes.

SGN Locus	Gene description ITAG3.0	NCBI Gene ID	Gene description NCBI RefSeq/1st or 2nd blastp hit	Fold-change	Total FPKM	Arabidopsis TAIR 10 Locus tag 1st and 2nd blastp hit
I versus H, UPREGULATED						
<b>Solyc03g006260</b>	Calcium-binding EF-hand (NCX)	101254062	sodium/calcium exchanger NCL1-like isoform X1	3.0	21.7	AT1G53210.1   AtNCL   sodium/calcium exchanger family protein; AT1G29025.1   Calcium-binding EF-hand family protein
<b>Solyc02g090560</b>	Calcium-transporting ATPase	101254450	calcium-transporting ATPase 12, plasma membrane-type-like	2.8	9.3	AT3G63380.1   ACA12   ATPase E1-E2 type family protein/haloacid dehalogenase-like hydrolase family protein ACA12; AT5G57110.2   ACA8, AT-ACA8   autoinhibited Ca <sup>2+</sup> -ATPase
<b>Solyc05g050360</b>	cyclic nucleotide gated channel 1 (CNGC)	101250508	cyclic nucleotide-gated ion channel 1-like	1.9	22.6	AT5G53130.1   CNGC1, ATCNGC1   cyclic nucleotide gated; AT4G01010.1   ATCNGC13, CNGC13   cyclic nucleotide-gated
<b>Solyc04g077870</b>	Calcium-transporting ATPase	101260132	calcium-transporting ATPase 1	1.6	27.1	AT1G27770.1   ACA1, PEA1   autoinhibited Ca <sup>2+</sup> -ATPase;
<b>Solyc08g023440</b>	Early-responsive to dehydration stress family	101268298	CSC1-like protein ERD4	1.5	40.5	AT4G37640.1   ACA2   calcium ATPase 2 AT1G30360.1   ERD4/OSCA3.1   CSC1-like protein ERD4 AT4G02900.1   OSCA1.7   ERD (early-responsive to dehydration stress)
I versus H, DOWNREGULATED						
<b>Solyc04g079910</b>	Calcium uniporter protein, mitochondrial	101249073	calcium uniporter protein 4, mitochondrial	9.1	3.8	AT2G23790   Protein of unknown function (DUF607); AT5G42610   Protein of unknown function (DUF607)
<b>Solyc06g006110</b>	vacuolar cation/proton exchanger (CAX)	101265339	vacuolar cation/proton exchanger 3-like	3.6	85.1	AT3G51860   CAX3, ATHCX1, CAX1-LIKE, ATCA3   cation exchanger; AT2G38170   CAX1, ATCA3, RCI4   cation exchanger
<b>Solyc09g072690</b>	Cation calcium exchanger (CCX)	101248713	cation/calcium exchanger 1, SLCX1	3.6	12.6	AT5G17860   CAX7   calcium exchanger 7; AT3G14070   CAX9, CCX3, ATCCX3   cation exchanger
<b>Solyc09g005260</b>	Vacuolar cation/proton exchanger 3 (CAX)	101254519	vacuolar cation/proton exchanger 3	3.2	381.9	AT3G51860   CAX3, ATHCX1, CAX1-LIKE, ATCA3   cation exchanger; AT2G38170   CAX1, ATCA3, RCI4   cation exchanger
<b>Solyc12g005400</b>	Cyclic nucleotide-gated ion channel, putative (CNGC)	101265895	cyclic nucleotide-gated ion channel 4	2.3	65.9	AT5G54250   ATCNGC4   cyclic nucleotide-gated channel
<b>Solyc10g006800</b>	Cyclic nucleotide-gated ion channel, putative (CNGC)	101246478	ref XP_004248279.1  PREDICTED: cyclic nucleotide-gated ion channel 4-like	2.0	30.7	AT5G54250   ATCNGC4   cyclic nucleotide-gated channel
<b>Solyc10g079300</b>	Calcium-transporting ATPase	101253440	putative calcium-transporting ATPase 11, plasma membrane-type	2.0	23.0	AT3G57330   ACA11   autoinhibited Ca <sup>2+</sup> -ATPase 11; AT2G41560   ACA4   autoinhibited Ca(2+)-ATPase, isoform
<b>Solyc11g069580</b>	Cyclic nucleotide-gated channel (CNGC)	101249432	protein CNGC15b	1.8	9.7	AT2G28260   ATCNGC15   cyclic nucleotide-gated channel; AT2G24610   ATCNGC14   cyclic nucleotide-gated channel
<b>Solyc04g076303</b>	Mechanosensitive ion channel-like protein	101254787	ref XP_010320208  mechanosensitive ion channel protein 3, chloroplastic isoform X1	1.6	48.0	AT1G58200   MSL3   MSCS-like 3
<b>Solyc12g088230</b>	mitochondrial malate dehydrogenase (?)	101254178	CSC1-like protein RXW8	1.6	13.5	AT1G58520   RXW8   lipases; hydrolases, acting on ester bond; AT1G10090   Early-responsive to dehydration stress

Ca<sup>2+</sup>/cation antiporters (CaCA), Ca<sup>2+</sup>-permeable channels and Ca<sup>2+</sup> ATPases are listed. Cyclic nucleotide-gated ion channels are included. Fold-change is the expression level ratio Infected/Healthy ( $q \leq 0.05$ ). Total FPKM corresponds to the sum of FPKM expression level of the corresponding gene in both samples. In brackets: symbol of transporter family.

necessary to generate sufficient turgor. Thus, a pivotal role is played by tonoplast-localized K<sup>+</sup>/H<sup>+</sup> antiporters, which are critical also for stomatal closure, vacuolar remodeling and control of vacuolar pH (Padmanaban et al., 2007; Andrés et al., 2014). Conspicuously, we observed an overall downregulation of K<sup>+</sup> and Na<sup>+</sup>/H<sup>+</sup> exchangers (like CHX20, CHX18-like and NHX1, as discussed in the following paragraph) in the infected midrib, which might mirror a similar regulation in the remainder of the leaf, in which it will be interesting to deepen their role in the control of stomatal conductance.

Chloroplasts are affected during almost all known plant-phytoplasma

interactions. In tomato, ‘Ca. P. solani’ infection causes massive disorganization of thylakoids and overall inhibition of genes related to light reactions and light harvesting (Buoso et al., 2019), which is associated with diminished photosynthesis (Fig. 1). Moreover, following phytoplasma infection, maintenance of K<sup>+</sup> and H<sup>+</sup> homeostasis in chloroplasts seems to be also crucial. Interestingly, we found that the chloroplastic K<sup>+</sup> antiporter 3, a homolog of Arabidopsis KEA3, was dramatically downregulated. AtKEA3 is a thylakoid K<sup>+</sup>/H<sup>+</sup> antiporter that contributes to the ΔpH component of the pmf (Wang and Shikanai, 2019). Silencing of AtKEA3 increases the luminal proton concentration and the

**Table 5**

Genes mediating Magnesium fluxes.

SGN Locus	Gene description ITAG3.0	NCBI Gene ID	Gene description NCBI RefSeq/1st or 2nd blastp hit	Fold- change	Total FPKM	Arabidopsis TAIR 10 Locus tag 1st and 2nd blastp hit
I versus H, DOWNREGULATED						
<b><i>Solyc11g066665</i></b>	Magnesium transporter MRS2-like protein	101267965	ref XP_004251000.1  PREDICTED: magnesium transporter MRS2-11, chloroplastic, X1	4.3	69.3	AT5G22830   ATMG10, GMN10, MG10, MRS2-11   magnesium transporter
<b><i>Solyc11g066660</i></b>	Magnesium transporter MRS2-like protein	101267965	magnesium transporter MRS2-11, chloroplastic	3.7	33.9	AT5G22830   ATMG10, GMN10, MG10, MRS2-11   magnesium transporter
<b><i>Solyc01g103760</i></b>	magnesium transporter NIPA (DUF803)	101246186	probable magnesium transporter NIPA4	1.8	13.3	AT1G71900   Protein of unknown function (DUF803)
<b><i>Solyc11g065090</i></b>	magnesium transporter NIPA (DUF803)	101264486	probable magnesium transporter NIPA6	1.8	48.5	AT1G34470   Protein of unknown function (DUF803)

Fold-change is the expression level ratio Infected/Healthy ( $q \leq 0.05$ ). Total FPKM corresponds to the sum of FPKM expression level of the corresponding gene in both samples. In italic, different SGN loci corresponding to the same Gene ID in NCBI annotation.

**Table 6**

Genes mediating Iron, Zinc and Manganese transport.

SGN Locus	Gene description ITAG3.0	NCBI Gene ID	Gene description NCBI RefSeq/ 1st or 2nd blastp hit	Fold- change	Total FPKM	Arabidopsis TAIR 10 Locus tag 1st and 2nd blastp hit
I versus H, UPREGULATED						
<b><i>Solyc01g006150</i></b>	Metal tolerance protein	101253924	metal tolerance protein 4-like	2.5	39.8	AT3G58060   MTP8   Cation efflux family protein
<b><i>Solyc03g082620</i></b>	Yellow stripe 1A transporter	101256566	metal-nicotianamine transporter YSL2	1.9	15.3	AT5G24380   YSL2, ATYSL2   YELLOW STRIPE like 2; AT5G53550   YSL3   YELLOW STRIPE like 3
I versus H, DOWNREGULATED						
<b><i>Solyc01g095510</i></b>	Mitochondrial carrier protein, putative	101267457	mitochondrial carrier protein MTM1	2.5	5.2	AT4G27940   ATMTM1, MTM1   manganese tracking factor
<b><i>Solyc03g007430</i></b>	Mitochondrial carrier protein, putative	101253663	mitochondrial carrier protein MTM1	2.3	22.0	AT4G27940   ATMTM1, MTM1   manganese tracking factor
<b><i>Solyc08g065190</i></b>	zinc transporter	101259773	zinc transporter 4, chloroplastic	2.0	66.8	AT1G10970   ZIP4, ATZIP4   zinc transporter 4 precursor; AT1G60960   IRT3, ATIRT3   iron regulated transporter
<b><i>Solyc03g116900</i></b>	Metal transporter	101246519	ref XP_004235940.2 metal transporter Nramp6	1.9	51.1	AT1G15960   NRAMP6, ATNRAMP6   NRAMP metal ion transporter; AT1G80830   NRAMP1, PMIT1, ATNRAMP1   natural resistance-associated macrophage protein
<b><i>Solyc01g100610</i></b>	Solute carrier family 40 member 3	101251418	solute carrier family 40 member 3, chloroplastic	1.7	17.2	AT5G26820   ATIREG3, MAR1, RTS3, IREG3   iron-regulated protein 3; AT5G03570   IREG2   iron regulated 2

Fold-change is the expression level ratio I/H ( $q \leq 0.05$ ). Total FPKM corresponds to the sum of FPKM expression level of the corresponding gene in both samples.

pH-dependent NPQ, and decreases the electron transport through the cytochrome *b<sub>6</sub>f* complex, with a detrimental effect on the overall photosynthesis capacity (Wang and Shikanai, 2019; Correa Galvis et al., 2020).

As reported above, anomalous accumulation of starch and soluble sugar in the leaf follows phytoplasma infection in several plants, including tomato, which showed also increased callose deposits occluding the ordinary sieve plates (Fig. 2; De Marco et al., 2016). When carbohydrates accumulate in leaves, photosynthesis becomes inhibited through a feedback mechanism (reviewed by Osorio et al., 2014), possibly explaining the decrease in net photosynthesis that we observed in tomato. However, a role in affecting photosynthetic net CO<sub>2</sub> assimilation might be played also by Mg<sup>2+</sup>, which decreased in the leaf lamina upon infection (Fig. 3). Mg<sup>2+</sup> is particularly critical for photosynthesis. In plant cells, up to 35% of Mg<sup>2+</sup> is preferentially allocated to chloroplast, where it acts as a cofactor for enzymes involved in C fixation and a constituent of the chlorophyll molecule (reviewed by Tian et al., 2021). In *Hordeum vulgare*, a reduced leaf Mg<sup>2+</sup> concentration was associated with a reduction of the CO<sub>2</sub> assimilation, prior to the light reactions (Jaghdani et al., 2021). Furthermore, a reduced Mg<sup>2+</sup> uptake in the chloroplast was closely associated with a decrease in ribulose 1, 5-bisphosphate carboxylase activity *in vivo* and a consequent decline in the photosynthetic rate in rice (Li et al., 2020). The same authors showed that Mg<sup>2+</sup> loading into rice chloroplasts is partly but notably

mediated by the chloroplast-envelope OsMGT3/OsMRS2-6 transporter. It is noteworthy that OsMRS2-6 is an ortholog of the tomato chloroplast MRS2-11, which was more than 4-fold downregulated in the infected midrib (Table 5). Taken together, our data suggest that the entire photosynthetic machinery seems compromised in *Ca. P. solani*-infected Micro-Tom midribs, where leaf chlorosis was associated with a dramatic alteration of chloroplast ultrastructure and an overall inhibition of genes related to photosynthetic light reactions, light harvesting, carotenoid biosynthesis, and porphyrin/chlorophyll metabolism (Buoso et al., 2019).

In infected tomato, leaf chlorosis and diminished net CO<sub>2</sub> fixation, as well as proliferation of witches' broom-like vegetative tissues, were observed together with sterility. It is possible that the reduced photosynthates have been diverged to alter vegetative architecture at the expense of flowers and fruits. Proliferation of vegetative tissues and sterile shoots represent phenotypic changes in plant hosts that favor their transmission to other trophic levels. Recently, decoupling of plant developmental phase transitions has been imputed to phytoplasma-produced effectors (Bai et al., 2009; Hoshi et al., 2009): in Arabidopsis, the effector SAP05 prolongs the host lifespan and induces bushiness and proliferation of sterile shoots by mediating the degradation of GATA and SPL transcription factors (Huang et al., 2021).

#### 4.2. Potassium, sodium and aquaporin-mediated transport is downregulated in midribs of infected plants

$K^+$  is the most abundant cellular cation, playing multiple vital roles in plants.  $K^+$  represents an osmoticum for cellular growth and stomatal function, crucially involved in cytosolic pH homeostasis and phloem solute transport. Several facilitator systems mediate the partitioning and recirculation of  $K^+$  among different tissues and organs. In Arabidopsis,  $K^+$  transporters and channels with low and high affinity have been described (Very and Sentenac, 2003). Most  $K^+$  absorbed by roots is released to the xylem (by Stelar  $K^+$  Outward Rectifier, SKOR, in Arabidopsis) and then transported to shoots with the transpiration stream (Gaymard et al., 1998; ). In shoots,  $K^+$  moves from the xylem to parenchyma cells via the apoplast; then,  $K^+$  follows the symplasmic route towards the phloem or, once effluxed from parenchyma cells, is loaded into the phloem to move to the shoot or return to the root. In the leaf midrib of infected tomato plants, the  $K^+$  concentration was lower when compared to healthy plants, whereas infected plants had higher  $K^+$  levels in roots. In parallel, stomatal conductance ( $g_s$ ) and leaf transpiration (E) were significantly decreased in infected plants. This result is consistent with a lower root-to-shoot translocation of  $K^+$  and/or a substantial relocation of  $K^+$  to roots from shoots following infection.

Examining the transcriptional changes of the phytoplasma-infected leaf midrib revealed an overall downregulation of  $K^+$  transporters, the localization and function of most of which is unknown, and *bona fide* inferred from their Arabidopsis homologs (Fig. 4; Supplemental Fig. S2). Concerning high-affinity transporters, we found that two genes of the KUP/HAK/KT family of symporters (Hyun et al., 2014) were repressed upon infection in the leaf midrib. Their Arabidopsis homologs (KUP6 and KUP8) play critical roles in osmotic adjustment by balancing  $K^+$  homeostasis in cell growth and drought stress responses in shoots (Osakabe et al., 2013). It is noteworthy that AtKUP6 is a target of the protein kinase SRK2E (SNF1-related protein kinases 2E), a key component of ABA signaling in the control of water stress responses (Osakabe et al., 2013). The activities of  $K^+$  channels and transporters are influenced by ABA (Pilot et al., 2003), whose concentration was reported to increase in leaves of different plant species infected by phytoplasmas (Bernardini et al., 2020). The KUP/HAK/KT family of transporters primarily mediate  $K^+$  fluxes, but some members play also important roles in  $Na^+$  fluxes. The  $Na^+/K^+$  ratio in tomato leaves did not significantly change following phytoplasma infection, as  $K^+$  and  $Na^+$  concentration decreased almost simultaneously (Fig. 3B). It is possible that the observed repression of some  $K^+$ ,  $Na^+$  and  $Na^+$  transporters (e.g., NHX1 and SIHKT1; 2) was aimed to control  $Na^+$  concentration in equilibrium with  $K^+$ . Besides its toxicity,  $Na^+$  can entry into the cytosol and cause membrane depolarization, which in turn hinders the inward  $K^+$  channel-mediated influx and promotes  $K^+$  efflux (Adams and Shin, 2014). For this reason, plants possess specific transporters that mediate  $Na^+$  efflux from the cytosol or  $Na^+$  retrieval and subsequent sequestration. The tomato SIHKT1; 2 belongs to the Trk/HKT family, which contains  $Na^+$  and  $K^+$  symporters functioning as  $Na^+$  uniporters at high external  $Na^+$  concentration in plant (Hamamoto et al., 2015). It was localized both in the xylem parenchyma cells, where mediates mostly the withdrawal of  $Na^+$  from the xylem (and subsequent compartmentation into the vacuoles) under salinity, and, possibly, in phloem-associated cells, where might mediate the phloem loading and redistribution to roots (Almeida et al., 2014; Jaime-Pérez et al., 2017). In our experimental conditions, which ensured optimal nutrient supply, the downregulation of SIHKT1;2 might explain the decrease in concentration of  $Na^+$  in the infected leaf midrib, aimed to control  $K^+$  and  $Na^+$  homeostasis. A prevented delivery of  $K^+$  and  $Na^+$  across the plasma membrane into the cytosol seems to be coordinated with other transporters, such as the proton exchangers NHX1 and CHXs, which should mediate their sequestration into vacuoles. The downregulation of all transporters described above would be consistent with a lower root-to-shoot translocation of  $K^+$ , more than a substantial relocation of

$K^+$  to roots from shoots following infection.

Concerning genes encoding antiporters, the most strongly down-regulated tomato gene was CHX20, a homolog of Arabidopsis AtCHX20 and AtCHX19. The cation/proton exchanger (CHX) family is largely unexplored and includes both  $K^+$  and  $Na^+$  antiporters in Arabidopsis. AtCHX17-20 belong to a group of electroneutral  $K^+/H^+$  exchangers that modulate  $K^+$  and pH homeostasis of distinct intracellular compartments (Chanroj et al., 2011). AtCHX19 is localized in the prevacuolar compartment (Chanroj et al., 2011), while AtCHX20 is an endomembrane  $K^+/H^+$  exchanger with a key role in light-induced stomatal opening: stomatal aperture of loss-of-function *chx20* mutants failed to fully open after light induction (Padmanaban et al., 2007). CHX family transporters are involved in  $K^+$  and  $Na^+$  transport, osmotic adjustment, stomatal opening, and salt tolerance (He and Huang, 2013; Sze et al., 2004; Isayenkov et al., 2020). The control of stomatal opening and closure also relies on the activities of NHXs, tonoplast-localized  $K^+$ ,  $Na^+/H^+$  exchangers that mediate the vacuolar accumulation of  $K^+$  in guard cells. Arabidopsis *nhx1-2 nhx2-1* double mutants showed reduced ability to create the vacuolar  $K^+$  pool, which, in turn, provoked greater  $K^+$  retention in the cytosol, impaired osmoregulation, and compromised turgor generation for cell expansion (Barragán et al., 2012; Andrés et al., 2014). Thus, tomato CHXs and NHXs might indirectly concur for the control of stomatal conductance, and their repression would be coherent with the physiological changes that we observed in the infected plants, assuming that their repression in the midrib may be mirrored by the rest of the leaf. Their localization in the different cell compartments and tissues will help to clarify their role in the response to phytoplasma infection. Regarding LeNHX1, higher gene expression was found in more tolerant species under salt stress (Gálvez et al., 2012). Together with LeNHX3 and LeNHX4, LeNHX1 belongs to the vacuolar clade of NHX transporters that, besides their protective function under salt or osmotic stress (Blumwald, 2000), play a significant role in  $K^+$  nutrition together with ion channels by mediating the  $K^+$  influx into vacuoles for cellular storage and turgor generation (Pardo et al., 2006; Isayenkov et al., 2020). As reported above, the maintenance of  $K^+$  and  $H^+$  homeostasis seems to be crucial also in chloroplasts. In Arabidopsis, the thylakoid  $K^+/H^+$  antiporter AtKEA3 contributes to the  $\Delta pH$  component of the pmf, with an effect on the overall photosynthesis efficiency (Wang and Shikanai, 2019; Correa Galvis et al., 2020). Interestingly, we found that the chloroplastic  $K^+$  antiporter 3, a homolog of Arabidopsis KEA3, was dramatically downregulated.

Potassium is necessary as counter-ion during anion absorption, especially nitrate which is one of the most abundant anion in plants (Engels and Marschner, 1993). We observed the dramatic down-regulation of three genes of the NITRATE TRANSPORTER 1/PEPTIDE TRANSPORTER FAMILY (NPF) of proteins in the infected midrib (Table 2). The tomato NRT1/PTR family 7.3 genes are orthologs of AtNRT1.5 (NPF7.3), which was initially identified as a nitrate or di/tripeptide transporter (Tsay et al., 2007) and later characterized as a proton-coupled  $H^+/K^+$  antiporter (Li et al., 2017). The mechanism of transport by NRT1.5 is still under debate, as this transporter affects the homeostatic balance between  $K^+$  and nitrate in the xylem stream and might thus function as a cotransporter of  $K^+$  and nitrate (Fig. 4). In fact, AtNRT1.5 was found to be downregulated under  $K^+$ -limited conditions, together with but independent of the  $K^+$  channel SKOR, probably to adjust the root-to-shoot  $K^+/NO_3^-$  transport to the level of  $K^+$  (Li et al., 2017). The same authors revealed that NRT1.5 is also involved in the coordination of  $K^+/NO_3^-$  distribution in plants (see Raddatz et al., 2020 for a review). Interestingly, recent studies into the Arabidopsis mutant *npf7.3*, the roots of which are not able to respond properly to gravity, and transport assays in yeast, have demonstrated that NPF7.3 can mediate indole-3-butyric acid uptake into the cells (Watanabe et al., 2020). The NRT1/PTR family includes a large number of members that are thought to transport numerous unidentified substrates and have multiple unknown functions (Tsay et al., 2007).

Fluxes of  $K^+$  are coupled to the activity of water channels/



aquaporins in the plasma membrane (PIPs). To cope with water deficiency, for example, rice plants were shown to downregulate  $K^+$  channels/transporters and water uptake mediated by PIPs (Liu et al., 2006). Five TIPs were downregulated in the leaf midrib upon phytoplasma infection, suggesting a similar coordination with genes mediating  $K^+$  fluxes in the midrib tissues. Analogously, two TIPs were downregulated. The tonoplast TIP2; 2 was shown to be a functional water transporter in tomato and overexpression resulted in improved fruit yield and plant biomass (Sade et al., 2009). Anyway, a growing body of evidence indicates that aquaporins are important regulators of plant-pathogen interaction, which ultimately lead to either plant immunity or pathogen virulence. The loss-of-function mutation at the AtPIP1; 4 gene locus not only nullifies the cytoplasmic import of pathogen- and PAMP-induced apoplastic  $H_2O_2$  but also cancels the subsequent immune responses, suggesting a pivotal role of AtPIP1; 4 in apo- and cytoplasmic signal transduction in immunity pathways (Tian et al., 2016).

#### 4.3. The transcriptional regulation of pumps, antiporters and channels concurs to the homeostasis of $Ca^{2+}$ in the leaf midrib

Calcium is an essential macronutrient in plants owing to its unique role as a messenger (Hirschi, 2004). Some environmental stimuli related to biotic or abiotic stresses cause  $Ca^{2+}$  losses in the extracellular space (cell wall, apoplast, rhizosphere), and simultaneously increases in cytosolic  $Ca^{2+}$  concentration ( $[Ca^{2+}]_{cyt}$ ). Oscillations of  $[Ca^{2+}]_{cyt}$  can induce gene expression or  $Ca^{2+}$  may bind to and activate other proteins like calmodulin or calcium-dependent protein kinases (Reddy et al., 2011; Sarwat et al., 2013). For this reason,  $Ca^{2+}$  influx and efflux, mediated by transporters and channels, are spatially and temporally regulated in a highly concerted manner. Rapid, transient variations in  $[Ca^{2+}]_{cyt}$  mostly rely on the activation of channels and transport proteins, evidenced in the present study by the transcriptional regulation of more than ten genes encoding channels, secondary transporters and pumps that might concur to the homeostasis of  $Ca^{2+}$  (Fig. 4; Supplemental Fig. S3).

Calcium in plants is taken up from the soil at the root tip and is later loaded into the xylem by specific transporters (White, 2001). Once  $Ca^{2+}$  reaches the leaves, it is no longer mobile (Pilbeam and Morley, 2007). In Arabidopsis and most dicots,  $Ca^{2+}$  preferentially accumulates within mesophyll cell vacuoles, and its concentration in the bundle sheath is low (Conn et al., 2011). The  $Ca^{2+}/H^+$  antiporters AtCAX3 and AtCAX1 are critical for sequestering  $Ca^{2+}$  into the vacuole, in coordination with channels that release  $Ca^{2+}$  (Conn et al., 2011). In our experiment we were unable to determine if the decrease in  $[Ca^{2+}]$  that we observed in the infected leaf midrib corresponded to a decrease in cytoplasmic or apoplastic  $[Ca^{2+}]$ , or variations in the phloem sap. However, two vacuolar CAX genes were more than 3-fold repressed by infection (Table 4). Conn et al. (2011) showed that *cax1/cax3* loss-of-function Arabidopsis mutant had a significantly lower mesophyll accumulation of  $Ca^{2+}$  compared to wild-type plants, paralleled by a three-fold higher  $[Ca^{2+}]$  in the apoplast, which in turn reduced stomatal conductance, photosynthetic capacity, and growth rate. Conversely, Park et al. (2005) demonstrated that fruits from tomato plants expressing Arabidopsis CAXs have more  $Ca^{2+}$  and a prolonged shelf life when compared to controls. The vacuolar compartmentation mediated by CAXs is essential to regulate apoplastic  $[Ca^{2+}]$  in order to optimize cell wall expansion, photosynthesis, transpiration and plant productivity, and mediate plant stress responses by the propagation of  $Ca^{2+}$  signals (Cheng et al., 2003, 2005; Zhao et al., 2008; Conn et al., 2011; Manohar et al., 2011). Moreover, CAXs play a key role in the storage of metals in the vacuoles of parenchyma cells. They mediate the sequestration of cations into the vacuole in antiport with  $H^+$ , thus utilizing the large proton electrochemical gradient across the tonoplast (Manohar et al., 2011). A broad substrate range characterizes CAXs, with the specificity depending on the amino acid sequence diversity among different CAXs (Shigaki et al., 2005; Shigaki and Hirschi, 2006). Anyway,  $Ca^{2+}$  transport is thought to

be a major role of the plant CAX transporters, the activity of which is a critical component in the maintenance of calcium nutrition. Thus, the repression of two vacuolar CAX genes seems consistent with the drop in  $[Ca^{2+}]$  in the infected leaf midrib, and might play also a role in the reduction of stomatal conductance we observed in the infected tomato. In addition, a role in regulating  $Ca^{2+}$  (and  $Na^+$ ) homeostasis might be assigned to the  $Na^+/Ca^{2+}$  exchanger SINCL1-like, which was upregulated in the infected midrib (Table 4). The Arabidopsis homolog AtNCL appeared to mediate  $Na^+$  vacuolar sequestration and  $Ca^{2+}$  release dependent from  $Ca^{2+}$  binding (Li et al., 2016).

$Ca^{2+}$  ATPases are localized at the plasma membrane, tonoplast, endoplasmic reticulum, and Golgi, where act as  $Ca^{2+}/H^+$  exchangers using directly ATP (Bonza and De Michelis, 2011).  $Ca^{2+}$  exchangers, such as CAXs, and  $Ca^{2+}$  ATPases proteins export  $Ca^{2+}$  from the cytosol primarily to the apoplast and the vacuole (Bonza and De Michelis, 2011). The concerted activity of these  $Ca^{2+}/H^+$  transporters determine both  $[Ca^{2+}]_{cyt}$  and  $pH_{cyt}$ , as  $pH_{cyt}$  strictly follows every change in  $[Ca^{2+}]_{cyt}$  (Behera et al., 2018). Together with CAXs, three  $Ca^{2+}$  ATPases were differently expressed in the infected midrib, and we hypothesize that such a regulation on both CAXs and differently localized  $Ca^{2+}$  ATPases might have a crucial role in determining changes in  $[Ca^{2+}]_{cyt}$  and signaling, as well as in controlling pH, in the response to phytoplasma infection. Noteworthy, two Arabidopsis tonoplast-localized pumps, ACA4 and ACA11 (ACA; auto-inhibited  $Ca^{2+}$  ATPase), were found to impact flg22-dependent  $Ca^{2+}$  signaling and trigger plant immunity (Hilleary et al., 2020).

Mechanosensitive channels are mechanosensors that gate the ion flow on mechanical stimuli. The OSCA/TMEM63 family of  $Ca^{2+}$  permeable stress-gated cation channels provide protection against osmotic shock and are also related to pathogen attack (Meisrimler et al., 2021). The first osmo-sensitive  $Ca^{2+}$  permeable cation channel proteins were identified in Arabidopsis by two independent research-groups, and named OSCA1 (*Arabidopsis thaliana* reduced hyperosmolality induced  $[Ca^{2+}]_i$  increase 1, alias OSCA1.1), and CSC1 (alias OSCA1.2), respectively (Yuan et al., 2014; Hou et al., 2014). CSC1 is a non-rectifying, plasma membrane-bound, calcium-permeable, and stress-gated cation channel, activated by hyperosmotic shock (Hou et al., 2014). CSC1 is permeable to  $Ca^{2+}$ ,  $K^+$  and  $Na^+$ , and its inactivation or closure is  $Ca^{2+}$ -dependent (Hou et al., 2014). Arabidopsis *osca1* loss-of-function mutants display a reduced  $Ca^{2+}$  elevation compared to wild-type plants when treated with osmotic stress agents like sorbitol (Yuan et al., 2014). The regulation of pressure-activated ion channels in tomato might suggest similar altered  $Ca^{2+}$  fluxes as a consequence of osmotic pressure changes in the infection site. Nucleotide-gated channels (CNGCs) are allosterically regulated by cytosolic signals such as cyclic nucleotides, calmodulin, and  $Ca^{2+}$ , and are not activated by the membrane potential. CNGCs can mediate  $Ca^{2+}$ ,  $K^+$  and in some cases  $Na^+$  fluxes (Pantoja, 2021). A truncated form of the plasma membrane AtCNGC1, for example, conferred  $Pb^{2+}$  tolerance to the plant, having lost the possibility of binding  $Pb^{2+}$  at the calmodulin binding site (Sunkar et al., 2000). No significant differences between the wild type and the transgenic lines were found in their content of a range of metals (Ca, K, Mg, Mn, Zn and Fe), suggesting that CNGC channels have only subtle effects on metal transport and are rather involved in signaling (Sunkar et al., 2000). The Arabidopsis CNGC4 is a calmodulin-gated calcium channel responsible for the cytosolic calcium burst required for PAMP-triggered immunity (PTI) in plants (Tian et al., 2019).

$Ca^{2+}$  influx from the apoplast (or into organelles) is facilitated by  $Ca^{2+}$ -permeable channels, whilst  $Ca^{2+}$  extrusion from the cytosol across the plasma membrane or into organelles is mediated by  $Ca^{2+}$  pumps and CaCA antiporters. Thus, the concomitant up- and downregulation of members of the same functional category might be explained with a localization in different cell types inside the leaf midrib (Fig. 4; Supplemental Fig. S3). As previously mentioned, phytoplasma infection impacts on transport in the phloem. Unfortunately, most of the DEGs that we found expressed in the leaf midrib are not characterized in

tomato, and hypotheses regarding as to which players are specifically critical at the phloem level are difficult to formulate. Regarding  $\text{Ca}^{2+}$  fluxes, however, it is known that phytoplasma infection triggers  $\text{Ca}^{2+}$  influx in *Vicia faba* sieve elements (Musetti et al., 2013), leading to their occlusion by callose deposition or protein sealing, and several channels/transporters among the DEGs are possible candidate in altering  $\text{Ca}^{2+}$  fluxes at the infection site. Bertazzon et al. (2019) reported that the signaling pathways, governed by  $\text{Ca}^{2+}$  and protein kinases, were significantly modulated in leaves of micro-propagated grapevine following Flavescence dorée phytoplasma infection. In particular, a decreased abundance of genes encoding receptor-like kinase (RLK) family proteins, calmodulin and calmodulin-like proteins and  $\text{Ca}^{2+}$  dependent protein kinases was observed. This could be consistent with the production and the consequent action of phytoplasma effectors on the host plant. In fact, effectors (i.e., SAP11, Sugio et al., 2011) were reported to affect plant hormonal pathways, which are modulated by  $\text{Ca}^{2+}$  signaling (Bethke et al., 1995).

#### 4.4. Phytoplasma infection alters the local distribution of Fe and Mn

Iron shifts to the phloem tissue from the surrounding tissue in the phytoplasma-infected tomato leaves and seems to sustain the pathogen metabolism, as an imposed Fe-deficiency reduces the phytoplasma titer (Buoso et al., 2019). This latter outcome seems paradoxical, as Fe is a potent generator of ROS (Pierre and Fontecave, 1999; Aznar et al., 2015), and signaling via ROS is widely considered to be central to disease resistance in plants (Torres, 2010). The formation of harmful hydroxyl radicals via the Fenton reaction is catalyzed by the free metal (Pierre and Fontecave, 1999), while in the phloem metals form stable complexes mainly with nicotianamine (NA), which is regarded as main chaperon for the long distance transportation and homeostasis of metals, including  $\text{Fe}^{2+}$  and  $\text{Mn}^{2+}$  (von Wiren et al., 1999). Moreover, the primary oxidative burst following pathogen recognition occurs in the apoplast (Torres, 2010), although high levels of ROS are produced when uncoupling or inhibition of photosynthesis and photorespiration occur in chloroplasts and peroxisomes (Karpinski et al., 2003). Accumulation of  $\text{Fe}^{2+}$  in the phloem prevalently in a chelated form, seems coherent with the expression of *SIYLS2*, encoding a transporter of metal-NA chelates which was upregulated in the infected leaf-midrib. *SIYLS2* is homologous to Arabidopsis *YSL2* and *YSL3*. Arabidopsis *YSL1*, *YSL2* and *YSL3* are plasma membrane transporters expressed in the vascular bundle parenchyma, where they mediate the (re)mobilization of Fe, Zn, and Cu in the form of metal-nicotianamine (NA) chelates from old leaves and the loading of these metals into inflorescences and seeds (DiDonato et al., 2004; Waters et al., 2006). *Oryza sativa YSL2* (*OsYSL2*), which belongs to the group of *SIYLS2* orthologs, is a functional  $\text{Fe}^{2+}$ - and  $\text{Mn}^{2+}$ -NA complex transporter that is expressed in phloem cells and developing seeds, where it is required for long-range transportation of  $\text{Fe}^{2+}$  and  $\text{Mn}^{2+}$  (Ishimaru et al., 2010). Thus, an enhanced  $\text{Fe}^{2+}$ -NA loading into the phloem mediated by *SIYLS2* is a likely scenario. In addition, an increase of Fe localized in the infection zone might be associated to compromised unloading and translocation, as the *CHLN* gene (Solyc01g100490), encoding a NA synthase (Ling et al., 1999), was downregulated in the phytoplasma-infected midrib (Buoso et al., 2019). The phytoplasma-infected Micro-Tom resembles the tomato NA-auxotroph mutant *chloronerva*, which is chlorotic, despite the presence of high concentration of Fe in its leaves, and fails to translocate Fe to young leaves and flowers (Ling et al., 1999; Stephan et al., 1990). Moreover, impaired long-distance translocation of  $\text{Fe}^{2+}$  may explain the drop in  $\text{Fe}^{2+}$  concentration that was observed in roots of the infected tomato plants (Buoso et al., 2019, Fig. 3). All these observations suggest that phytoplasma-infected phloem is a strong sink for Fe. For specific members of the *YSL* family a biological role in the innate immunity of plants can be considered. Chen et al. (2014) demonstrated that the expression of *YLS3* in Arabidopsis is induced by salicylate and that the *ysl3* mutant increases its susceptibility against *Pseudomonas syringae* pv.

tomato (*Pst*) DC3000.

The increase of  $\text{Fe}^{2+}$  in the infected midrib was accompanied by a significant drop in  $\text{Mn}^{2+}$ , resembling data reported by Rossi et al. (2010) who observed an  $\text{Fe}^{2+}/\text{Mn}^{2+}$  imbalance in phytoplasma infected pear leaves. The transcript profile of genes putatively related to metal ion transport appeared to be coherent with the compromised  $\text{Mn}^{2+}$  (and  $\text{Fe}^{2+}$ ) homeostasis in the infected midrib. In particular, we observed a downregulation of *SINRAMP6* together with the induction of a *MTP* gene. NRAMP proteins are broad range membrane-bound metal transporters (Curie et al., 2000) which may have evolved as proton-metal cotransporters to ensure the metal import under thermodynamically unfavorable conditions (Pittman, 2005). Arabidopsis NRAMP1 is the major high-affinity Mn transporter (Cailliatte et al., 2010), which acts in concert with the high-affinity Fe transporter IRT1 to take up  $\text{Fe}^{2+}$  into roots under iron-replete conditions (Castaings et al., 2016). *AtNRAMP6* localizes to a vesicular-shaped endomembrane compartment distinct from the vacuole, functioning as intracellular metal (mainly Cd) transporter (Cailliatte et al., 2009). NRAMPs are also involved in the defense against pathogens. The Arabidopsis *nramp3 nramp4* double mutant is impaired in the accumulation of reactive oxygen species and ferritin, a Fe storage protein, resulting in increased susceptibility to the bacterial pathogen *Erwinia chrysanthemi* (Segond et al., 2009). MTPs (also called CDFs: Cation Diffusion Facilitators) are specific for  $\text{Mn}^{2+}$  transport (Peiter et al., 2007). The Arabidopsis homolog MTP8 is a root vacuole  $\text{Mn}^{2+}$  transporter that prevents plants from  $\text{Mn}^{2+}$  toxicity in Fe-deficiency conditions, in which the poorly substrate-specific  $\text{Fe}^{2+}$  transporter IRT1 causes  $\text{Mn}^{2+}$  overload (Eroglu et al., 2016). Moreover, MTP8 increases the vacuole-stored  $\text{Mn}^{2+}$  pool in the seed embryo, and contributes to the  $\text{Mn}^{2+}$  homeostasis by creating a vacuolar sink favorable for  $\text{Mn}^{2+}$  accumulation (Eroglu et al., 2017). Anyway, MTP8 can mediate also  $\text{Fe}^{2+}$  sequestration into the vacuole, being part of a module of tonoplast transporters (including the NRAMP3/NRAMP4 and VIT1) regulating  $\text{Fe}^{2+}$  and  $\text{Mn}^{2+}$  homeostasis in seed (Eroglu et al., 2017). The opposite transcriptional regulation of a NRAMP and a MTP member in the tomato midrib might represent an attempt to control the changes in the concentration of the two free metals in different cell compartments, and overcome the loss of  $\text{Mn}^{2+}$  and/or  $\text{Fe}^{2+}$  ion in the tissues surrounding the infection site.

#### 4.5. Phytoplasma invasion of sieve elements impacts nutrient fluxes

Symptoms of phytoplasma-diseased plants are similar to those associated with diverse nutritional and mineral imbalances (Schweikofler et al., 2008; Buoso et al., 2019; Ermacora and Osler, 2019). The transcriptional response of phytoplasma-infected tomato midrib-enriched leaves indicated robust regulation of several genes involved in transmembrane transport of highly diverse molecules, not only mineral nutrients (Supplemental Tables S2–S4), consistently with altered accumulation of amino acids, organic acids, and secondary metabolites, as previously reported in phytoplasma-infected plants (Choi et al., 2004; Srivastava et al., 2014; Prezelj et al., 2016). Excessive starch accumulation in the chloroplasts as well as impaired phloem sugar transport were shown in ‘Ca. P. solani’-infected tomato (De Marco et al., 2016, 2021; Buoso et al., 2019), and grapevine (Santi et al., 2013a, b). Altered sugar translocation would be corroborated by the down-regulation of several both sugar cotransporters and uniporters of the SWEET (Sugar Will Eventually be Exported Transporter) family in the infected midrib (Supplemental Table S2). Anomalous deposits of callose ( $\beta$ -1,3-glucan) occluding the sieve plates and formation of phloem protein aggregates were also observed (Fig. 2, De Marco et al., 2016, 2021; Buoso et al., 2019). Moreover, morphological alteration such as cell wall thickening and distortion at phloem level were reported to occur in infected tomato maintained in both soil (De Marco et al., 2016) and in hydroponics (Fig. 2), which might concur to alter phloem transport. Thickening of the cell walls could be associated with a reduction of sugar translocation, and subsequent sugar accumulation in form of other

polysaccharides (i.e., cellulose) in source organs (Marschner, 1995). An increase in reactive oxygen species (ROS) and peroxidase, which bind phenolic compounds and wall glycoproteins, may also cause wall stiffening (Tenhaken, 2015). Indeed, photosynthesis is inhibited and stomatal conductance decreased without a rapid removal of photosynthates. Obstructions in phloem transport, together with a reduced loading of photosynthates should alter the turgor pressure and affect the local and long-distance transport to shoot and root sinks of not only photosynthates, but also peptides, proteins, and other macromolecules, as well as electrical signals, phytohormones, metabolites (Koenig and Hoffmann-Benning, 2020) and mineral nutrients. In the case of  $K^+$ , the downregulation of several  $K^+$  transporters and water channels, associated with a reduced  $K^+$  content in the leaf midrib, would be consistent with a lower root-to-shoot translocation of  $K^+$  throughout the transpiration stream, together with a reduced relocation throughout the phloem and the apoplast to roots. Analysis of the most up- and down-regulated transport-related genes in the transcriptomic profile revealed a generally reduced translocation of nutrients in diseased plants (Supplemental Tables S2 and S4). Anyway, in the case of micronutrients such as Fe, the phytoplasma-infected phloem seems to be a strong sink (herein, Buoso et al., 2019), so we cannot exclude that phytoplasma might compete for nutrients locally, and/or target transport players directly. Moreover, we cannot exclude that phytoplasma presence in root phloem (Supplemental Table S1) might impact on the delivery of water and nutrient throughout the xylem.

In conclusion, the response to phytoplasma includes significant changes in the homeostasis of ions such as  $K^+$ ,  $Ca^{2+}$ ,  $Mg^{2+}$ ,  $Fe^{2+}$  and  $Mn^{2+}$ , and dramatic alterations in the expression of related transmembrane transporters in the host plant. It is noteworthy that the transcriptional response involves several ion transporters putatively targeted to subcellular compartments. If transporters localized at the plant cell plasma membrane control metal ion uptake and release, those localized in endogenous subcellular compartments are mainly responsible for sequestration and remobilization of metal ions in the cell. In particular, the central vacuole appears to be important for the regulation of metal homeostasis, as both a sub-cellular sink and a source, such as for the propagation of  $Ca^{2+}$  signals. Regarding chloroplast, altered fluxes of almost all examined ions and inferred by gene expression of localized transporters might be associated to the dramatic disorganization of thylakoids, and the compromised photosynthetic apparatus in the phytoplasma-infected leaves (Buoso et al., 2019). Future efforts deserve to be directed toward a detailed characterization and localization of the best candidate genes provided by the present study.

#### CRedit authorship contribution statement

SB and SS designed experiments; SB performed ICP-OES and gene expression surveys; SS carried out RNA-seq data analysis with FM; RM performed TEM observations; AC collected gas exchange data. SS conceived and supervised the project. SS wrote the article with inputs from RM and WS.

#### Declaration of competing interest

The authors declare that they have no known competing financial interests or personal relationships that could have appeared to influence the work reported in this paper.

#### Acknowledgements

RNA sequencing was performed by IGA Technologies Service, Udine, Italy. Most of bioinformatics work was carried at the CyVerse cyberinfrastructure ([www.cyverse.org](http://www.cyverse.org)), which is supported by the USA National Science Foundation's Directorate for Biological Sciences. This work was supported by FFABR\_2017 (Italian MIUR) and RICLIB funds to SS and by an Academia Sinica Investigator Award to WS.

#### Appendix A. Supplementary data

Supplementary data to this article can be found online at <https://doi.org/10.1016/j.jplph.2022.153659>.

#### References

- Adams, E., Shin, R., 2014. Transport, signaling, and homeostasis of potassium and sodium in plants. *J. Integr. Plant Biol.* 56, 231–249. <https://doi.org/10.1111/jipb.12159>.
- Al-Ghaithi, A.G., Hanif, M.A., Al-Busaidi, W.M., et al., 2016. Increased sodium and fluctuations in minerals in acid limes expressing witches' broom symptoms. *SpringerPlus* 5, 418. <https://doi.org/10.1186/s40064-016-2049-0>.
- Almeida, P., de Boer, G., de Boer, A.H., 2014. Differences in shoot  $Na^+$  accumulation between two tomato species are due to differences in ion affinity of HKT1;2. *J. Plant Physiol.* 171, 438–447.
- Andrés, Z., Pérez-Hormaeche, J., Leidi, E.O., Schlücking, K., Steinhörst, L., McLachlan, D. H., Schumacher, K., Hetherington, A., Kudla, J., Cubero, B., Pardo, J.M., 2014. Control of vacuolar dynamics and regulation of stomatal aperture by tonoplast potassium uptake. *Proc. Natl. Acad. Sci. Unit. States Am.* 111 (17), E1806–E1814. <https://doi.org/10.1073/pnas.1320421111>.
- Aznar, A., Chen, N.W., Thomine, S., Dellagi, A., 2015. Immunity to plant pathogens and iron homeostasis. *Plant Sci.* 240, 90–97.
- Bai, X., Correa, V.R., Toruño, T.Y., Ammar, E.D., Kamoun, S., Hogenhout, S.A., 2009. AY-WB phytoplasma secretes a protein that targets plant cell nuclei. *MPMI (Mol. Plant-Microbe Interact.)* 22, 18–30. <https://doi.org/10.1094/MPMI-22-1-0018>.
- Bai, X., Zhang, J., Ewing, A., Miller, S.A., Radek, A.J., Shevchenko, D.V., Tsukerman, K., Walunas, T., Lapidus, A., Campbell, J.W., Hogenhout, S.A., 2006. Living with genome instability: the adaptation of phytoplasmas to diverse environments of their insect and plant hosts. *J. Bacteriol.* 188, 3682–3696. <https://doi.org/10.1128/JB.188.10.3682-3696.2006>.
- Barragán, V., Leidi, E.O., Andrés, Z., Rubio, L., De Luca, A., Fernández, J.A., Cubero, B., Pardo, J.M., 2012. Ion exchangers NHX1 and NHX2 mediate active potassium uptake into vacuoles to regulate cell turgor and stomatal function in Arabidopsis. *Plant Cell* 24 (3), 1127–1142. <https://doi.org/10.1105/tpc.111.095273>.
- Behera, S., Zhaolong, X., Luoni, L., Bonza, M.C., Doccula, F.G., De Michelis, M.I., Morris, R.J., Schwarzländer, M., Costa, A., 2018. Cellular  $Ca^{2+}$  signals generate defined pH signatures in plants. *Plant Cell* 30 (11), 2704–2719. <https://doi.org/10.1105/tpc.18.00655>, 2018.
- Bernardini, C., Pagliari, L., De Rosa, V., Almeida-Trapp, M., Santi, S., Martini, M., Buoso, S., Loschi, A., Loi, N., Chiesa, F., Mithöfer, A., van Bel, A.J.E., Musetti, R., 2020. Pre-symptomatic modified phytohormone profile is associated with lower phytoplasma titres in an Arabidopsis seor1ko line. *Sci. Rep.* 10 (1), 1–16. <https://doi.org/10.1038/s41598-020-71660-0>.
- Bertamini, M., Nedunchezian, N., 2001. Effects of phytoplasma [stolbur-subgroup (Bois noir-BN)] on photosynthetic pigments, saccharides, ribulose 1, 5-bisphosphate carboxylase, nitrate and nitrite reductases, and photosynthetic activities in field-grown grapevine (*Vitis vinifera* L. cv. Chardonnay) leaves. *Photosynthetica* 39 (1), 119–122. <https://doi.org/10.1023/A:1012412406727>.
- Bertazzon, N., Bagnaresi, P., Forte, V., Mazzucotelli, E., Filippin, L., Guerra, D., Zechini, A., Cattivelli, L., Angelini, E., 2019. Grapevine comparative early transcriptomic profiling suggests that Flavescence dorée phytoplasma represses plant responses induced by vector feeding in susceptible varieties. *BMC Genom.* 20, 526, 2019.
- Bethke, P.C., Gilroy, S., Jones, R.L., 1995. Calcium and plant hormone action. In: Davies, P.J. (Ed.), *Plant Hormones*. Springer, Dordrecht, Germany. [https://doi.org/10.1007/978-94-011-0473-9\\_14](https://doi.org/10.1007/978-94-011-0473-9_14).
- Bienfait, H.F., van den Briel, W., Mesland-Mul, N.T., 1985. Free space iron pools in roots: generation and mobilization. *Plant Physiol.* 78, 596–600. <https://doi.org/10.1104/pp.78.3.596>.
- Blum, M., Chang, H., Chuguransky, S., Grego, T., Kandasamy, S., Mitchell, A., Nuka, G., Paysan-Lafosse, T., Qureshi, M., Raj, S., Richardson, L., Salazar, G.A., Williams, L., Bork, P., Bridge, A., Gough, J., Haft, D.H., Letunic, I., Marchler-Bauer, A., Mi, H., Natale, D.A., Necci, M., Orengo, C.A., Pandurangan, A.P., Rivoire, C., Sigrist, C.J.A., Sillitoe, I., Thanki, N., Thomas, P.D., Tosatto, S.C.E., Wu, C.H., Bateman, A., Finn, R. D., 2020. The InterPro protein families and domains database: 20 years on. *Nucleic Acids Res.* 48 (D1), D344–D354. <https://doi.org/10.1093/nar/gkaa977>, 49.
- Blumwald, E., 2000. Sodium transport and salt tolerance in plants. *Curr. Opin. Cell Biol.* 12, 431–434.
- Bonza, M.C., De Michelis, M.I., 2011. The plant  $Ca^{2+}$ -ATPase repertoire: biochemical features and physiological functions. *Plant Biol (Stuttg)* 13, 421–430. <https://doi.org/10.1111/j.1438-8677.2010.00405.x>.
- Buoso, S., Pagliari, L., Musetti, R., Martini, M., Marroni, F., Schmidt, W., Santi, S., 2019. 'Candidatus Phytoplasma solani' interferes with the distribution and uptake of iron in tomato. *BMC Genom.* 20 (1), 1–21. <https://doi.org/10.1186/s12864-019-6062-x>.
- Cabot, C., Martos, S., Llugany, M., Gallego, B., Tolrà, R., Poschenrieder, C.A., 2019. Role for zinc in plant defense against pathogens and herbivores. *Front. Plant Sci.* 4, 1171. <https://doi.org/10.3389/fpls.2019.01171>.
- Cai, X., Lyttton, J., 2004. The cation/ $Ca^{2+}$  exchanger super family: phylogenetic analysis and structural implications. *Mol. Biol. Evol.* 9, 1692–1703. <https://doi.org/10.1093/molbev/msh177>.
- Cailliatte, R., Lapeyre, B., Briat, J.F., Mari, S., Curie, C., 2009. The NRAMP6 metal transporter contributes to cadmium toxicity. *Biochem. J.* 422 (2), 217–228. <https://doi.org/10.1042/BJ20090655>.



- Cailliatte, R., Schikora, A., Briat, J.-F., Mari, S., Curie, C., 2010. High-affinity manganese uptake by the metal transporter NRAMP1 is essential for Arabidopsis growth in low manganese conditions. *Plant Cell* 22, 904–917.
- Castaignes, L., Caquot, A., Loubet, S., et al., 2016. The high-affinity metal transporters NRAMP1 and IRT1 team up to take up iron under sufficient metal provision. *Sci. Rep.* 6, 37222. <https://doi.org/10.1038/srep37222>.
- Chanroj, S., Lu, Y., Padmanaban, S., Nanatani, K., Uozumi, N., Rao, R., Sze, H., 2011. Plant-specific cation/H<sup>+</sup> exchanger 17 and its homologs are endomembrane K<sup>+</sup> transporters with roles in protein sorting. *J. Biol. Chem.* 30 (39), 33931–33941. <https://doi.org/10.1074/jbc.M111.252650>, 286.
- Chen, C.-C., Chien, W.-F., Lin, N.-C., Yeh, K.-C., 2014. Alternative functions of Arabidopsis YELLOW STRIPE-LIKE3: from metal translocation to pathogen defense. *PLoS One* 9 (5), e98008. <https://doi.org/10.1371/journal.pone.0098008>.
- Cheng, N.-H., Pittman, J.K., Barkla, B.J., Shigaki, T., Hirschi, K.D., 2003. The Arabidopsis cax1 mutant exhibits impaired ion homeostasis, development, and hormonal responses and reveals interplay among vacuolar transporters. *Plant Cell* 15, 347–364.
- Cheng, N.-H., Pittman, J.K., Shigaki, T., Lachmansingh, J., LeClere, S., Lahner, B., Salt, D. E., Hirschi, K.D., 2005. Functional association of Arabidopsis CAX1 and CAX3 is required for normal growth and ion homeostasis. *Plant Physiol.* 138, 2048–2060.
- Choi, Y.H., Tapias, E.C., Kim, H.K., Lefebvre, A.W., Erkelens, C., Verhoeven, J.T.J., Brzin, J., Zel, J., Verpoorte, R., 2004. Metabolic discrimination of Catharanthus roseus leaves infected by phytoplasma using 1H-NMR spectroscopy and multivariate data analysis. *Plant Physiol.* 135 (4), 2398–2410. <https://doi.org/10.1104/pp.104.041012>.
- Conn, S.J., Gillham, M., Athman, A., Schreiber, A.W., Baumann, U., Moller, I., Cheng, N.-H., Stancombe, M.A., Hirschi, K.D., Webb, A.R., Burton, R., Kaiser, B.N., Tyerman, S. D., Leigh, R.A., 2011. Cell specific vacuolar calcium compartmentation regulates apoplastic calcium concentration, gas exchange and plant productivity. *Plant Cell* 23, 240–257. <https://doi.org/10.1105/tpc.109.072769>.
- Correa Galvis, V., Strand, D.D., Messer, M., Thiele, W., Bethmann, S., Hübner, D., Uflewski, M., Kaiser, E., Siemiakowska, B., Morris, B.A., Tóth, S.Z., Watanabe, M., Brückner, F., Höfgen, R., Jahns, P., Schöttler, M.A., Armbruster, U., 2020. H<sup>+</sup> transport by K<sup>+</sup> EXCHANGE ANTIPORTER3 promotes photosynthesis and growth in chloroplast ATP synthase mutants. *Plant Physiol.* 182 (4), 2126–2142. <https://doi.org/10.1104/pp.19.01561>.
- Curie, C., Alonso, J.M., Le Jean, M., Ecker, J.R., Briat, J.F., 2000. Involvement of NRAMP1 from Arabidopsis thaliana in iron transport. *Biochem. J.* 347, 749–755.
- De Marco, F., Pagliari, L., Degola, F., Buxa, S.V., Loschi, A., Dinant, S., Le Hir, R., Morin, H., Santi, S., Musetti, R., 2016. Combined microscopy and molecular analyses show phloem occlusions and cell wall modifications in tomato leaves in response to *Candidatus* Phytoplasma solani. *J. Microsc.* 263, 212–225. <https://doi.org/10.1111/jmi.12426>.
- De Marco, F., Batailler, B., Thorpe, M.R., Razan, F., Rozenn, L.E., Vilaine, F., Bouchereau, A., Martin-Magniette, M.-L., Eveillard, S., Dinant, S., 2021. Involvement of SUT1 and SUT2 sugar transporters in the impairment of sugar transport and changes in phloem exudate contents in phytoplasma-infected plants. *Int. J. Mol. Sci.* 22 (2), 745. <https://doi.org/10.3390/ijms22020745>.
- DiDonato Jr., R.J., Roberts, L.A., Sanderson, T., Easley, R.B., Walker, E.L., 2004. Arabidopsis Yellow Stripe-Like2 (YSL2): a metal-regulated gene encoding a plasma membrane transporter of nicotianamine-metal complexes. *Plant J.* 39 (3), 403–414. <https://doi.org/10.1111/j.1365-3113.2004.02128.x>. PMID: 15255869.
- Endeshaw, S.T., Murolo, S., Romanazzi, G., Neri, D., 2012. Effects of Bois noir on carbon assimilation, transpiration, stomatal conductance of leaves and yield of grapevine (*Vitis vinifera*) cv. Chardonnay. *Physiol. Plantarum* 145, 286–295. <https://doi.org/10.1111/j.1399-3054.2012.01576.x>.
- Engels, C., Marschner, H., 1993. Influence of the form of nitrogen supply on root uptake and translocation of cations in the xylem exudate of maize (*Zea mays* L.). *J. Exp. Bot.* 44, 1695–1701. <https://doi.org/10.1093/jxb/44.11.1695>.
- Ermacor, P., Osler, R., 2019. Symptoms of phytoplasma disease. *Methods Mol. Biol.* 1875, 53–67. [https://doi.org/10.1007/978-1-4939-8837-2\\_5](https://doi.org/10.1007/978-1-4939-8837-2_5). PMID: 30361995.
- Eroglu, S., Giehl, R., Meier, B., Takahashi, M., Terada, Y., Ignatyev, K., Andresen, E., Küpper, H., Peiter, E., von Wirén, N., 2017. Metal tolerance protein 8 mediates manganese homeostasis and iron reallocation during seed development and germination. *Plant Physiol.* 174 (3), 1633–1647. <https://doi.org/10.1104/pp.16.01646>.
- Eroglu, S., Meier, B., von Wirén, N., Peiter, E., 2016. The vacuolar manganese transporter MTP8 determines tolerance to iron deficiency-induced chlorosis in Arabidopsis. *Plant Physiol.* 170 (2), 1030–1045. <https://doi.org/10.1104/pp.15.01194>.
- Fetter, K., Van Wilder, V., Moshelion, M., Chaumon, F., 2004. Interactions between plasma membrane aquaporins modulate their water channel activity. *Plant Cell* 16 (1), 215–228. <https://doi.org/10.1105/tpc.017194>.
- Gálvez, F.J., Baghour, M., Hao, G., Cagnac, O., Rodríguez-Rosales, M.P., Venema, K., 2012. Expression of LeNHX isoforms in response to salt stress in salt sensitive and salt tolerant tomato species. *Plant Physiol. Biochem.* 51, 109–115. <https://doi.org/10.1016/j.plaphy.2011.10.012>. Epub 2011 Oct 28. PMID: 22153246.
- Gaymard, F., Pilot, G., Lacombe, B., Bouchez, D., Bruneau, D., Boucherez, J., et al., 1998. Identification and disruption of a plant shaker-like outward channel involved in (K<sup>+</sup>) release into the xylem sap. *Cell* 94, 647–655. [https://doi.org/10.1016/s0092-8674\(00\)81606-2](https://doi.org/10.1016/s0092-8674(00)81606-2).
- Hamamoto, S., Horie, T., Hauser, F., Deinlein, U., Schroeder, J.I., Uozumi, N., 2015. HKT transporters mediate salt stress resistance in plants: from structure and function to the field. *Curr. Opin. Biotechnol.* 32, 113–120. <https://doi.org/10.1016/j.copbio.2014.11.025>. Epub 2014 Dec 18. PMID: 25528276.
- He, Z., Huang, Z., 2013. Expression analysis of LeNHX1 gene in mycorrhizal tomato under salt stress. *J. Microbiol.* 51 (1) <https://doi.org/10.1007/s12275-013-2423-3>, 100–4.
- Hilleary, R., Paez-Valencia, J., Vens, C., Toyota, M., Palmgren, M., Gilroy, S., 2020. Tonoplast-localized Ca<sup>2+</sup> pumps regulate Ca<sup>2+</sup> signals during pattern-triggered immunity in *Arabidopsis thaliana*. *Proc. Natl. Acad. Sci. U.S.A.* 117 (31), 18849–18857. <https://doi.org/10.1073/pnas.2004183117>.
- Hirschi, K.D., 2004. The calcium conundrum. Both versatile nutrient and specific signal. *Plant Physiol.* 136, 2438–2442. <https://doi.org/10.1104/pp.104.04649>.
- Hoshi, A., Oshima, K., Kakizawa, S., Ishii, Y., Ozeki, J., Hashimoto, M., Komatsu, K., Kagiwada, S., Yamaji, Y., Namba, S., 2009. A unique virulence factor for proliferation and dwarfism in plants identified from a phytopathogenic bacterium. *Proc. Natl. Acad. Sci. U.S.A.* 106, 6416–6421. <https://doi.org/10.1073/pnas.0813038106>.
- Hou, C., Tian, W., Kleist, T., et al., 2014. DUF221 proteins are a family of osmosensitive calcium-permeable cation channels conserved across eukaryotes. *Cell Res.* 24, 632–635. <https://doi.org/10.1038/cr.2014.14>.
- Huang, W., MacLean, A.M., Sugio, A., Maqbool, A., Busscher, M., Cho, S.T., Kamoun, S., Kuo, C.H., Immink, R.G.H., Hogenhout, S.A., 2021. Parasitic modulation of host development by ubiquitin-independent protein degradation. *Cell* 184 (20), 5201–5214.e12. <https://doi.org/10.1016/j.cell.2021.08.029>.
- Hyun, T.K., Rim, Y., Kim, E., Kim, J.-S., 2014. Genome-wide and molecular evolution analyses of the KT/HAK/KUP family in tomato (*Solanum lycopersicum* L.). *Genes* 5, 365–374. <https://doi.org/10.1007/s12258-014-0174-0>.
- Isayenkova, S.V., Dabrovolski, S.A., Pan, T., Shabala, S., 2020. Phylogenetic diversity and physiological roles of plant monovalent cation/H<sup>+</sup> antiporters. *Front. Plant Science* 11, 573564. <https://doi.org/10.3389/fpls.2020.573564>.
- Ishimaru, Y., Masuda, H., Bashir, K., Inoue, H., Tsukamoto, T., Takahashi, M., Nakanishi, H., Aoki, N., Hirose, T., Ohsugi, R., Nishizawa, N.K., 2010. Rice metal-nicotianamine transporter, OsYSL2, is required for the long-distance transport of iron and manganese. *Plant J.* 62, 379–390. <https://doi.org/10.1111/j.1365-3113.2010.04158.x>.
- Jaghiani, S.J., Jahns, P., Trankner, M., 2021. Mg deficiency induces photo-oxidative stress primarily by limiting CO<sub>2</sub> assimilation and not by limiting photosynthetic light utilization. *Plant Sci.* 302, 110751.
- Jaime-Pérez, N., Pineda, B., García-Sogo, B., Atores, A., Athman, A., Byrt, C.S., Olías, R., Asins, M.J., Gilliam, M., Moreno, V., Belver, A., 2017. The sodium transporter encoded by the HKT1;2 gene modulates sodium/potassium homeostasis in tomato shoots under salinity. *Plant Cell Environ.* 40 (5), 658–671. <https://doi.org/10.1111/pce.12883>.
- Kanehisa, M., Goto, S., Furumichi, M., Tanabe, M., Hirakawa, M., 2010. KEGG for representation and analysis of molecular networks involving diseases and drugs. *Nucleic Acids Res.* 38, D355–D360. <https://doi.org/10.1093/nar/gkp896>.
- Karpinski, S., Gabrys, H., Mateo, A., Karpinska, B., Mullineaux, P.M., 2003. Light perception in plant disease defence signalling. *Curr. Opin. Plant Biol.* 6, 390–396.
- Kim, D., Perte, G., Trapnell, C., Pimentel, H., Kelley, R., Salzberg, S.L., 2013. TopHat2: accurate alignment of transcriptomes in the presence of insertions, deletions and gene fusions. *Genome Biol.* 14 <https://doi.org/10.1186/gb-2013-14-4-r36>. R36.
- Koenig, A.M., Hoffmann-Benning, S., 2020. The interplay of phloem-mobile signals in plant development and stress response. *Biosci. Rep.* 40 (10) <https://doi.org/10.1042/BSR20193329>. BSR20193329.
- Kube, M., Mitrovic, J., Duduk, B., Rabus, R., Seemüller, E., 2012. Current view on phytoplasma genomes and encoded metabolism. *Sci. World J.* 25, 185942. <https://doi.org/10.1100/2012/185942>.
- Kube, M., Siewert, C., Migdoll, A.M., Duduk, B., Holz, S., Rabus, R., Seemüller, E., Mitrovic, J., Müller, I., Büttner, C., Reinhardt, R., 2014. Analysis of the complete genomes of *Acholeplasma brassicae*, *A. palmiae* and *A. laidlawii* and their comparison to the obligate parasites from *Candidatus* phytoplasma. *J. Mol. Microbiol. Biotechnol.* 24 (1), 19–36. <https://doi.org/10.1159/000354322>.
- Lee, S., Chu, C.-Y., Chu, C.-C., 2021. Variability of phytoplasma infection density in *Poinsettia* and evaluation of its association with the level of branching in host plants. *Plant Dis.* 105, 1539–1545.
- Lepka, P., Stitt, M., Moll, E., Seemüller, E., 1999. Effect of phytoplasmal infection on concentration and translocation of carbohydrates and amino acids in periwinkle and tobacco. *Physiol. Mol. Plant Pathol.* 55, 59–68. <https://doi.org/10.1006/pmpp.1999.0202>.
- Li, J., Yokosho, K., Liu, S., Cao, H.R., Yamaji, N., Zhu, X.G., Liao, H., Ma, J.F., Chen, Z.C., 2020. Diel magnesium fluctuations in chloroplasts contribute to photosynthesis in rice. *Nature Plants* 6, 848–859.
- Li, H., Yu, M., Du, X.Q., Wang, Z.F., Wu, W.H., Quintero, F.J., Jin, X.H., Li, H.D., Wang, Y., 2017. NRT1.5/NPF7.3 Functions as a Proton-Coupled H<sup>+</sup>/K<sup>+</sup> Antiporter for K<sup>+</sup> Loading into the Xylem in Arabidopsis. *Plant Cell* 29 (8), 2016–2026. <https://doi.org/10.1105/tpc.16.00972>.
- Li, P., Zhang, G., Gonzales, N., Guo, Y., Hu, H., Park, S., Zhao, J., 2016. Ca(2+)-regulated and diurnal rhythm-regulated Na(+)/Ca(2+) exchanger AtNCL affects flowering time and auxin signalling in Arabidopsis. *Plant Cell Environ.* 39 (2), 377–392. <https://doi.org/10.1111/pce.12620>.
- Ling, H.Q., Koch, G., Bäumlein, H., Ganai, M.W., 1999. Map-based cloning of chloronerva, a gene involved in iron uptake of higher plants encoding nicotianamine synthase. *Proc. Natl. Acad. Sci. U.S.A.* 96, 7098–7103. <https://doi.org/10.1073/pnas.96.12.7098>.
- Liu, H.-Y., Liu Sun, W.-N., Su, W.-A., Tang, Z.-C., 2006. Co-regulation of water channels and potassium channels in rice. *Physiol. Plantarum* 128, 58–69.
- Lu, P., Outlaw Jr., W.H., Smith, B.G., Freed, G.A., 1997. A new mechanism for the regulation of stomatal aperture size in intact leaves (accumulation of mesophyll-



- derived sucrose in the guard-cell wall of *Vicia faba*). *Plant Physiol.* 114 (1), 109–118. <https://doi.org/10.1104/pp.114.1.109>.
- MacRobbie, E.A., 2006. Osmotic effects on vacuolar ion release in guard cells. *Proc. Natl. Acad. Sci. U.S.A.* 103 (4), 1135–1140. <https://doi.org/10.1073/pnas.0510023103>.
- Maehijima, K., Oshima, K., Namba, S., 2014. Exploring the phytoplasmas, plant pathogenic bacteria. *J. Gen. Plant Pathol.* 80, 210–221. <https://doi.org/10.1007/s10327-014-0512-8>.
- Manohar, M., Shigaki, T., Hirschi, K.D., 2011. Plant cation/H<sup>+</sup> exchangers (CAEs): biological functions and genetic manipulations. *Plant Biol.* 13, 561–569. <https://doi.org/10.1111/j.1438-8677.2011.00466.x>.
- Marschner, H., 1995. *Mineral Nutrition of Higher Plants*, second ed. 889pp. Academic Press, London, U.K.
- Meisrimler, C.-N., Allan, C., Eccersall, S., Morris, R.J., 2021. Interior design: how plant pathogens optimize their living conditions. *New Phytol.* 229, 2514–2524. <https://doi.org/10.1111/nph.17024>.
- Mi, H., Muruganujan, A., Ebert, D., Huang, X., Thomas, P.D., 2019. PANTHER version 14: more genomes, a new PANTHER GO-slim and improvements in enrichment analysis tools. *Nucleic Acids Res.* 47 (D1), D419–D426. <https://doi.org/10.1093/nar/gky1038>. PMID: 30407594; PMCID: PMC6323939.
- Musetti, R., Buxa, S.V., De Marco, F., Loschi, A., Polizzotto, R., Kogel, K.H., van Bel, A.J., 2013. Phytoplasma-triggered Ca<sup>2+</sup> influx is involved in sieve-tube blockage. *Mol. Plant Microbe Interact.* 26, 379–386. <https://doi.org/10.1094/MPMI-08-12-0207-R>.
- Musetti, R., Marabottini, R., Badiani, M., Martini, M., di Toppi, L.S., Borselli, S., Borgo, M., Osler, R., 2007. On the role of H<sub>2</sub>O<sub>2</sub> in the recovery of grapevine (*Vitis vinifera* cv. Prosecco) from Flavescence dorée disease. *Funct. Plant Biol.* 34, 750–758. <https://doi.org/10.1071/FP06308>.
- Osakabe, Y., Arinaga, N., Umezawa, T., Katsura, S., Nagamachi, K., Tanaka, H., Ohiraki, H., Yamada, K., Seo, S.U., Abo, M., Yoshimura, E., Shinozaki, K., Yamaguchi-Shinozaki, K., 2013. Osmotic stress responses and plant growth controlled by potassium transporters in *Arabidopsis*. *Plant Cell* 25 (2), 609–624. <https://doi.org/10.1105/tpc.112.105700>.
- Oshima, K., Kakizawa, S., Nishigawa, H., Jung, H.Y., Wei, W., Suzuki, S., Arashida, R., Nakata, D., Miyata, S., Ugaki, M., Namba, S., 2004. Reductive evolution suggested from the complete genome sequence of a plant-pathogenic phytoplasma. *Nat. Genet.* 36 (1), 27–29. <https://doi.org/10.1038/ng1277>.
- Osorio, S., Ruan, Y.L., Fernie, A.R., 2014. An update on source-to-sink carbon partitioning in tomato. *Front. Plant Sci.* 5, 516. <https://www.frontiersin.org/article/10.3389/fpls.2014.00516>.
- Outlaw, W.H., 2003. Integration of cellular and physiological functions of guard cells. *Crit. Rev. Plant Sci.* 22, 503–529. <https://doi.org/10.1080/713608316>.
- Padmanaban, S., Chanroj, S., Kwak, J.M., Li, X., Ward, J.M., Sze, H., 2007. Participation of endomembrane cation/H<sup>+</sup> exchanger AtCHX20 in osmoregulation of guard cells. *Plant Physiol.* 144, 82–93. <https://doi.org/10.1104/pp.106.092155>.
- Pagliari, L., Buoso, S., Santi, S., Furch, A.C., Martini, M., Degola, F., Loschi, A., van Bel, A.J.E., Musetti, R., 2017. Filamentous sieve element proteins are able to limit phloem mass flow, but not phytoplasma spread. *J. Exp. Bot.* 68, 3673–3688. <https://doi.org/10.1093/jxb/erx199>.
- Pantoja, O., 2021. Recent advances in the physiology of ion channels in plants. *Annu. Rev. Plant Biol.* 72, 463–495. <https://doi.org/10.1146/annurev-arplant-081519-035925>. Epub 2021 Jan 11. PMID: 33428476.
- Pardo, J.M., Cubero, B., Leidi, E.O., Quintero, F.J., 2006. Alkali cation exchangers: roles in cellular homeostasis and stress tolerance. *J. Exp. Bot.* 57, 1181–1199. <https://doi.org/10.1093/jxb/erj114>.
- Park, S., Cheng, N.H., Pittman, J.K., Yoo, K.S., Park, J., Smith, R.H., Hirschi, K.D., 2005. Increased calcium levels and prolonged shelf life in tomatoes expressing *Arabidopsis* H<sup>+</sup>/Ca<sup>2+</sup> transporters. *Plant Physiol.* 139 (3), 1194–1206. <https://doi.org/10.1104/pp.105.066266>.
- Peiter, E., Montanini, B., Gobert, A., Pedas, P., Husted, S., Maathuis, F.J., Blaudez, D., Chalot, M., Sanders, D., 2007. A secretory pathway-localized cation diffusion facilitator confers plant manganese tolerance. *Proc. Natl. Acad. Sci. USA* 104 (20), 8532–8537. <https://doi.org/10.1073/pnas.0609507104>.
- Pierre, J.L., Fontecave, M., 1999. Iron and activated oxygen species in biology: the basic chemistry. *Biomolecules* 12, 195–199.
- Pilbeam, D.J., Morley, P.S., 2007. Calcium. In: Barker, V.A., Pilbeam, J.D. (Eds.), *Handbook of Plant Nutrition*. CRC Press, Taylor and Francis Group, Boca Raton, pp. 121–144.
- Pilot, G., Gaymard, F., Mouline, K., Chérel, I., Sentenac, H., 2003. Regulated expression of *Arabidopsis* Shaker K<sup>+</sup> channel genes involved in K<sup>+</sup> uptake and distribution in the plant. *Plant Mol. Biol.* 51 (5), 773–787.
- Pittman, J.K., 2005. Managing the manganese: molecular mechanisms of manganese transport and homeostasis. *New Phytol.* 167, 733–742. <https://doi.org/10.1111/j.1469-8137.2005.01453.x>.
- Prezelj, N., Covington, E., Roitsch, T., Gruden, K., Fragner, L., Weckwerth, W., Chersicola, M., Vodopivec, M., Dermastia, M., 2016. Metabolic consequences of infection of grapevine (*Vitis vinifera* L.) cv. "Modra frankinja" with Flavescence dorée phytoplasma. *Front. Plant Sci.* 7, 711. <https://doi.org/10.3389/fpls.2016.00711>.
- Quaglino, F., Zhao, Y., Casati, P., Bulgari, D., Bianco, P.A., Wei, W., Davis, R.E., 2013. 'Candidatus *Phytoplasma solani*', a novel taxon associated with stolbur and bois noir-related diseases of plants. *Int. J. Syst. Evol. Microb.* 63, 2879–2894. <https://doi.org/10.1099/ijs.0.044750-0>.
- Raddatz, N., Morales de los Ríos, L., Lindahl, M., Quintero, F.J., Pardo, J.M., 2020. Coordinated Transport of Nitrate, Potassium, and Sodium. *Front. Plant Sci.* 11, 247. <https://doi.org/10.3389/fpls.2020.00247>.
- Reddy, A.S., Ali, G.S., Celesnik, H., Day, I.S., 2011. Coping with stresses: roles of calcium and calcium/calmodulin-regulated gene expression. *Plant Cell* 23 (6), 2010–2032. <https://doi.org/10.1105/tpc.111.084988>.
- Reuscher, S., Akiyama, M., Mori, C., Aoki, K., Shibata, D., Shiratake, K., 2013. Genome-wide identification and expression analysis of aquaporins in tomato. *PLoS One* 19 (11), e79052. <https://doi.org/10.1371/journal.pone.0079052>, 8.
- Rossi, G., Beni, C., Socciarelli, S., Marconi, S., Pastore, M., Del Vaglio, M., Gervasi, F., 2010. Mineral nutrition of pear and apricot trees cultivated in Southern Italy area damaged by phytoplasma microorganisms. *Acta Hort.* 868, 433–438.
- Sade, N., Vinocur, B.J., Diber, A., Shatil, A., Ronen, G., Nissan, H., Wallach, R., Karchi, H., Moshelion, M., 2009. Improving plant stress tolerance and yield production: is the tonoplast aquaporin SLP2;2 a key to isohydric to anisohydric conversion. *New Phytol.* 181 (3), 651–661. <https://doi.org/10.1111/j.1469-8137.2008.02689.x>.
- Saier Jr., M.H., Tran, C.V., Barabote, R.D., 2006. TCDB: the Transporter Classification Database for membrane transport protein analyses and information. *Nucleic Acids Res.* 34, D181–D186.
- Santi, S., De Marco, F., Polizzotto, R., Grisan, S., Musetti, R., 2013a. Recovery from stolbur disease in grapevine involves changes in sugar transport and metabolism. *Front. Plant Sci.* 4, 171–182. <https://doi.org/10.3389/fpls.2013.00171>.
- Santi, S., Grisan, S., Pierascio, A., De Marco, F., Musetti, R., 2013b. Laser microdissection of grapevine leaf phloem infected by stolbur reveals site-specific gene responses associated to sucrose transport and metabolism. *Plant Cell Environ.* 36 (2), 343–355. <https://doi.org/10.1111/j.1365-3040.2012.02577>.
- Sarwat, M., Ahmad, P., Nabi, G., Hu, X., 2013. Ca(2+) signals: the versatile decoders of environmental cues. *Crit. Rev. Biotechnol.* 33 (1), 97–109. <https://doi.org/10.3109/07388551.2012.672398>.
- Schweiggler, W., Cassar, A., Stimpf, E., 2008. Reduced levels of calcium and other mineral elements in grapevine leaves affected by Bois noir (BN). *Mitt. Klosterneub.* 58, 117–122.
- Segond, D., Dellagi, A., Lanquar, V., Rigault, M., Patrit, O., Thomine, S., Expert, D., 2009. NRAMP genes function in *Arabidopsis thaliana* resistance to *Erwinia chrysanthemi* infection. *Plant J.* 58 (2), 195–207. <https://doi.org/10.1111/j.1365-3113.2008.03775.x>. Epub 2008 Dec 11. PMID: 19121106.
- Shigaki, T., Barkla, B.J., Miranda-Vergara, M.C., Zhao, J., Pantoja, O., Hirschi, K.D., 2005. Identification of a crucial histidine involved in metal transport activity in the *Arabidopsis* cation/H<sup>+</sup> exchanger CAX1. *J. Biol. Chem.* 280, 30136–30142.
- Shigaki, T., Hirschi, K.D., 2006. Diverse functions and molecular properties Emerging for CAX cation/H<sup>+</sup> exchangers in plants. *Plant Biol.* 8, 419–429. <https://doi.org/10.1055/s-2006-923950>.
- Srivastava, S., Pandey, R., Kumar, S., Nautiyal, C.S., 2014. Correspondence between flowers and leaves in terpenoid indole alkaloid metabolism of the phytoplasma-infected *Catharanthus roseus* plants. *Protoplasma* 251 (6), 1307–1320. <https://doi.org/10.1007/s00709-014-0621-4>.
- Stephan, U.W., Scholz, G., Rudolph, A., 1990. Distribution of nicotianamine, a presumed symplast ion transporter, in different organs of sunflower and of a tomato wild type and its mutant chloronerva. *Biochem. Physiol. Pflanz. (BPP)* 186, 81–88.
- Sze, H., Padmanaban, S., Cellier, F., Honys, D., Cheng, N.-H., Bock, K.W., Conéjéro, G., Li, X., Twell, D., Ward, J.M., Hirschi, K., 2004. Expression patterns of a novel AtCHX gene family highlight potential roles in osmotic adjustment and K<sup>+</sup> homeostasis in pollen development. *Plant Physiol.* 136, 2532–2547. <https://doi.org/10.1104/pp.104.046003>.
- Sugio, A., Maclean, A.M., Kingdom, H.N., Grieve, V.M., Manimekalai, R., Hogenhout, S.A., 2011. Diverse targets of phytoplasma effectors: from plant development to defense against insects. *Annu. Rev. Phytopathol.* 49, 175–195.
- Sunkar, R., Kaplan, B., Bouché, N., Arazi, T., Dolev, D., Talke, I.N., Maathuis, F.J., Sanders, D., Bouchez, D., Fromm, H., 2000. Expression of a truncated tobacco NtCBP4 channel in transgenic plants and disruption of the homologous *Arabidopsis* GNGC1 gene confer Pb<sup>2+</sup> tolerance. *Plant J.* 24 (4), 533–542. <https://doi.org/10.1046/j.1365-3113.2000.00901.x>. PMID: 11115134.
- Talbott, L.D., Zeiger, E., 1998. The role of sucrose in guard cell osmoregulation. *J. Exp. Bot.* 329–337. <https://www.jstor.org/stable/23695966>.
- Tenhaken, R., 2015. Cell wall remodeling under abiotic stress. *Front. Plant Sci.* 5, 771. <https://doi.org/10.3389/fpls.2014.00771>.
- Tian, S., Wang, X., Li, P., Wang, H., Ji, H., Xie, J., Qiu, Q., Shen, D., Dong, H., 2016. Plant aquaporin AtPIP1;4 links apoplastic H<sub>2</sub>O<sub>2</sub> induction to disease immunity pathways. *Plant Physiol.* 171 (3), 1635–1650. <https://doi.org/10.1104/pp.15.01237>.
- Thor, K., 2019. Calcium—Nutrient and Messenger. *Front. Plant Sci.* 10, 440. <https://doi.org/10.3389/fpls.2019.00440>.
- Tian, X.Y., He, D.D., Bai, S., Zeng, W.Z., Wang, Z., Wang, M., Wu, L.Q., Chen, Z.C., 2021. Physiological and molecular advances in magnesium nutrition of plants. *Plant Soil* 468, 1–17. <https://doi.org/10.1007/s11104-021-05139-w>.
- Tian, W., Hou, C., Ren, Z., Wang, C., Zhao, F., Dahlbeck, D., Hu, S., Zhang, L., Niu, Q., Li, L., Staskiewicz, B.J., Luan, S., 2019. A calmodulin-gated calcium channel links pathogen patterns to plant immunity. *Nature* 572 (7767), 131–135. <https://doi.org/10.1038/s41586-019-1413-y>.
- Trapnell, C., Hendrickson, D.G., Sauvageau, M., Goff, L., Rinn, J.L., Pachter, L., 2013. Differential analysis of gene regulation at transcript resolution with RNA-seq. *Nat. Biotechnol.* 31, 46. <https://doi.org/10.1038/nbt.2450>.
- Torres, M.A., 2010. ROS in biotic interactions. *Physiol. Plantarum* 138, 414–429. <https://doi.org/10.1111/j.1399-3054.2009.01326.x>.
- Tsay, Y.F., Chiu, C.C., Tsai, C.B., C. Ho, C.H., Hsu, P.K. 2007. Nitrate transporters and peptide transporters. *FEBS Lett.*, 581, 2290–2300.
- USEPA. 1995. EPA Method 3052: Microwave Assisted Acid Digestion of Siliceous and Organically Based Matrices. in: *Test Methods for Evaluating Solid Waste*. 3rd Edn. Washington, DC.

- van Bel, A.J.E., Musetti, R., 2019. Sieve element biology provides leads for research on phytoplasma lifestyle in plant hosts. *J. Exp. Bot.* 70, 3737–3755. <https://doi.org/10.1093/jxb/erz172>.
- Very, A.A., Sentenac, H., 2003. Molecular mechanisms and regulation of K<sup>+</sup> transport in higher plants. *Annu. Rev. Plant Biol.* 54, 575–603. <https://doi.org/10.1146/annurev.arplant.54.031902.134831>.
- Vitali, M., Chitarra, W., Galetto, L., Bosco, D., Marzachi, C., Gullino, M.L., Spanna, F., Lovisolo, C., 2013. Flavescence dorée phytoplasma deregulates stomatal control of photosynthesis in *Vitis vinifera*. *Ann. Appl. Biol.* 162 (3), 335–346. <https://doi.org/10.1111/aab.12025>.
- von Caemmerer, S., Lawson, T., Oxborough, K., Baker, N.R., Andrews, T.J., Raines, C.A., 2004. Stomatal conductance does not correlate with photosynthetic capacity in transgenic tobacco with reduced amounts of Rubisco. *J. Exp. Bot.* 55 (400), 1157–1166. <https://doi.org/10.1093/jxb/erh128>.
- von Wiren, N., Klair, S., Bansal, S., Briat, J.F., Khodr, H., Shioiri, T., Leigh, R.A., Hider, R. C., 1999. Nicotianamine chelates both Fe<sup>III</sup> and Fe<sup>II</sup>. Implications for metal transport in plants. *Plant Physiol.* 119 (3), 1107–1114. <https://doi.org/10.1104/pp.119.3.1107>.
- Wang, C., Shikanai, T., 2019. Modification of activity of the thylakoid H<sup>+</sup>/K<sup>+</sup> antiporter KEA3 disturbs ΔpH-Dependent regulation of photosynthesis. *Plant Physiol.* 181 (2), 762–773. <https://doi.org/10.1104/pp.19.00766>.
- Watanabe, S., Takahashi, N., Kanno, Y., Suzuki, H., Aoi, Y., Takeda-Kamiya, N., Toyooka, K., Kasahara, H., Hayashi, K.I., Umeda, M., Seo, M., 2020. The *Arabidopsis* NRT1/PTR FAMILY protein NPF7.3/NRT1.5 is an indole-3-butyric acid transporter involved in root gravitropism. *Proc. Natl. Acad. Sci. U. S. A.* 8;117(49):31500–31509. doi: 10.1073/pnas.2013305117.
- Waters, B.M., Chu, H.-H., Didonato, R.J., Roberts, L.A., Easley, R.B., Lahner, B., Salt, D.E., Walker, E.L., 2006. Mutations in *Arabidopsis* yellow stripe-like1 and yellow stripe-like3 reveal their roles in metal ion homeostasis and loading of metal ions in seeds. *Plant Physiol.* 141 (4), 1446–1458. <https://doi.org/10.1104/pp.106.082586>.
- White, P.J., 2001. The pathways of calcium movement to the xylem. *J. Exp. Bot.* 52 (358), 891–899. <https://doi.org/10.1093/jexbot/52.358.891>.
- Yuan, F., Yang, H., Xue, Y., Kong, D., Ye, R., et al., 2014. OSCA1 mediates osmotic-stress-evoked Ca<sup>2+</sup> increases vital for osmosensing in *Arabidopsis*. *Nature* 514 (7522), 367–371.
- Zhao, J., Barkla, B.J., Marshall, J., Pittman, J.K., Hirschi, K.D., 2008. The *Arabidopsis* cax3 mutants display altered salt tolerance, pH sensitivity and reduced plasma membrane H<sup>+</sup>-ATPase activity. *Planta* 227, 659–669.
- Zhao, J., Liu, M.J., 2009. Variation of mineral element contents in Chinese jujube with witches' broom disease. *Acta Hort.* 840, 399–404.

## Further reading

- Mosimann, M., Goshima, S., Wenzler, T., Lüscher, A., Uozumi, N., Mäser, P.A., 2010. Trk/HKT-type K<sup>+</sup> transporter from *Trypanosoma brucei*. *Eukaryot. Cell* 9 (4), 539–546. <https://doi.org/10.1128/EC.00314-09>.